A SIMPLE QUADRATIC NODAL MODEL FOR HEXAGONAL GEOMETRY

by

Youssef A. Shatilla

B.S., Nuclear Engineering
Alexandria University, Egypt (1985)

M.S., Nuclear Engineering
Alexandria University, Egypt (1988)

Submitted to the Department of Nuclear Engineering

in Partial Fulfillment of the Requirements

for the Degree of

DOCTOR OF SCIENCE

at the

MASSACHUSETTS INSTITUTE OF TECHNOLOGY

September 1992

Signature of Author _____
Department of Nuclear Engineering, August 28, 1992

Certified by _____
Professor Allan F. Henry
Thesis Supervisor

Accepted by _____
Professor Allan F. Henry
Chairman, Committee on Graduate Students

A SIMPLE QUADRATIC NODAL MODEL FOR HEXAGONAL GEOMETRY

by
Youssef A. Shatilla

Submitted to the Department of Nuclear Engineering
on August 7, 1992 in partial fulfillment of the
requirements of the Degree of Doctor of Science in
the field of Nuclear Engineering

ABSTRACT

The objective of this research was to develop and implement a method for analyzing three-dimensional static and transient behavior of reactors composed of regular hexagonal subregions in radial planes with thermal-hydraulic feedback option.

A nodal method for analyzing reactors composed of hexagonal subregions in radial planes is described. Within each hexagon the shapes of transverse integrated group-fluxes are approximated as quadratic polynomials. Discontinuity factors are introduced to account for this approximation and for approximations made in replacing physically heterogeneous nodes by "equivalent" homogeneous regions. A simple, constant pressure, one-dimensional (parallel channel) thermal-hydraulic model is also incorporated.

Numerical comparisons with static reference calculations indicate that, without the use of discontinuity factors, the method provides predictions of nodal fluxes and global eigenvalue that are slightly less accurate than those obtained using somewhat more complicated nodal model and much more accurate than finite difference model with one mesh cube per node. Additional test comparisons suggest that discontinuity factors obtained from infinite lattice calculations are marginally acceptable for small, heavy water moderated and reflected cores composed of heterogeneous subassemblies. The thermal-hydraulic feedback option of the model is proven to work properly and provides excellent agreement with other nodal methods in Cartesian geometry.

Numerical comparisons with transient reference calculations indicate that the method is consistent in predicting the behavior of large heavy water reactors. Its thermal-hydraulic feedback option yields an excellent agreement with Cartesian geometry nodal methods. However, the method is slower than other nodal methods primarily because of the relatively higher number of unknowns per node per energy modeled and because no special acceleration procedures were applied.

Thesis Supervisor: Allan F. Henry
Title: Professor of Nuclear Engineering

ACKNOWLEDGMENTS

ALLAH is the First and the Last to be thanked for His mercy and blessings on me without which this work would have never seen the light.

I would like to extend my sincere gratitude to my thesis supervisor, Professor Allan F. Henry, for his excellent guidance during the course of this investigation. His pleasant character has always been a catalyst for finishing this work with the least hardship and agony.

Thanks are also due to Professor David D. Lanning, who served as my thesis reader, for his continuous encouragement and technical support.

The prayers of my mother and the support of my father, sister, and brother have always kept me going forward and never backward.

The financial support of this research by the Department of Energy is gratefully acknowledged.

TABLE OF CONTENTS

Page

Abstract 2

Acknowledgements 3

Table of Contents 4

List of Figures 7

List of Tables 8

Chapter (1) INTRODUCTION 9

1.1 Overview and Motivation 9
1.2 Background 10
1.2.1 Homogenization Methods 10
1.2.2 Nodal Diffusion Methods 11
1.3 Objective of the Present Research 15
1.4 Thesis Structure 16

Chapter (2) SOLUTION OF THE STATIC NEUTRON DIFFUSION EQUATION 18

2.1 Introduction 18
2.2 Derivation of the Nodal Equations 20
2.2.1 Triangular-Shaped-Node Model 23
2.2.2 Hexagonal-Shaped-Node Model 25
2.2.3 Evaluation of Discontinuity Factors 32
2.3 Boundary Conditions 34
2.4 Thermal-Hydraulic Feedback Model 36
2.4.1 The WIGL Model 36
2.4.2 Cross Section Feedback 39
2.5 Summary 40

TABLE OF CONTENTS
(continued)

Page

Chapter (3) NUMERICAL SOLUTION METHOD FOR THE STATIC NEUTRON DIFFUSION EQUATION AND APPLICATIONS..... 41

3.1 Introduction..... 41
3.2 Numerical Properties..... 42
3.2.1 Triangular-Shaped-Node Model..... 42
3.2.2 Hexagonal-Shaped-Node Model..... 47
3.3 Applications..... 56
3.3.1 Applications without Thermal-Hydraulic Feedback..... 56
3.3.2 Applications with Thermal-Hydraulic Feedback..... 63
3.4 Summary..... 66

Chapter (4) SOLUTION OF THE DYNAMIC NEUTRON DIFFUSION EQUATION..... 68

4.1 Introduction..... 68
4.2 Derivation of the Time-Dependent Nodal Equations..... 69
4.3 Thermal-Hydraulic Feedback Model..... 76
4.3.1 The WIGL Model..... 76
4.3.2 Cross Section Feedback..... 78
4.4 Summary..... 79

Chapter (5) NUMERICAL SOLUTION METHOD FOR THE DYNAMIC NEUTRON DIFFUSION EQUATION AND APPLICATIONS..... 80

TABLE OF CONTENTS
(continued)

Page

5.1 Introduction 80
5.2 Numerical Properties 81
5.3 Numerical Solution Scheme 86
5.4 Applications 89
5.4.1 Applications without Thermal-Hydraulic Feedback 89
5.4.2 Applications with Thermal-Hydraulic Feedback 93
5.5 Summary 94

Chapter (6) SUMMARY AND CONCLUSIONS 95

6.1 Summary 95
6.2 Conclusions and Recommendations 97

REFERENCES 99

Appendix A MATERIAL SPECIFICATIONS (Static Applications) 103

Appendix B MATERIAL SPECIFICATIONS (Transient Applications) 110

LIST OF FIGURES

Figure	Title	Page
1.1	An overview of a typical cross sectional area of a "K- reactor"	14
2.1	Examples of the notation used in the derivation of the nodal equations	22
2.2	Two neighboring hexagonal nodes.	26
2.3	Smallest repeating subregion of the SRS reactors. The arrows represent the relationships between currents.	35
2.4	Triangular mesh used in reference and infinite-lattice calculations.	35
2.5	Two typical thermal-hydraulic nodes for plutonium and tritium production	38
3.1	Flow diagram of iterative solution method (from Gehin, 1990)	48
3.2	Flow diagram of iterative solution method	55
3.3	ANL-Mark22 reactor geometry and material specifications	58
3.4	Cross sectional area of the core used for the benchmark problem	60
3.5	One-dimensional problem results	62
3.6	Power density vs. axial distance	64
3.7	Power densities vs. radial distance (power fluctuations)	65
3.8	One-dimensional problem results (with feedback)	66
5.1	Flow diagram of iterative solution method.	88
5.2	Joshua reactor geometry and material specifications	90
5.3	Normalized thermal flux vs. time for Joshua problem	92
5.4	20-F^0-degree decrease in the coolant inlet temperature	94

LIST OF TABLES

Table	Title	Page
2.1	Values of α and β for standard boundary conditions	36
3.1	Accuracy of various models as applied to the simulation of a heavy water production reactor (From Shatilla and Henry, 1992)	57
3.2	Comparisons of quadratic and finite-difference results (From Shatilla and Henry, 1992)	61

CHAPTER ONE

INTRODUCTION

1.1 Overview and Motivation

The safe operation of a nuclear reactor requires the accurate prediction of its neutron population at all time for all possible conditions and configurations. Although this might look as straightforward as solving a set of differential equations that govern the neutron behavior in a reactor, in real life the picture is somewhat more complicated than this. The reason is that the problem is non-linear: neutron behavior is affected by the thermal conditions while thermal hydraulic analysis of the reactor requires accurate information concerning the neutron flux distribution.

Traditionally, reactor neutronic analysis is done using few group diffusion theory with fine-mesh, finite-difference solution techniques. However, constraints on problem size (large number of mesh spacings needed) and angular behavior (diffusion theory not valid) are major drawbacks of the finite-difference method. These have been overcome by now well-known techniques. The first problem can be overcome by using nodal techniques (Smith, 1979 and Lawrence et al., 1978) and the second one can be overcome by using modern homogenization methods (Henry, 1975) which

introduce "homogenized" diffusion theory parameters to represent the heterogeneous nodes of a reactor.

Although the world nuclear industry is primarily based on light water reactors of Cartesian geometry, the hexagonal lattice is very attractive for many advanced reactor concepts like liquid metal fast breeder reactors, modular high temperature gas cooled reactors, and heavy water moderated reactors. Although results will be applicable to a broad class of reactors composed of hexagonal assemblies, the primary emphasis of this thesis is directed towards the analysis of heavy water reactors such as those located in the Savannah River Site. The objective will be to develop a nodal method requiring the use of only one mesh point per hexagon in a hexagonal plane, yet capable of providing an accurate simulation of three-dimensional, transient power behavior.

1.2 Background

1.2.1 Homogenization Methods

A basic assumption of diffusion theory is that the neutron angular distribution is, at most, linearly anisotropic. This assumption is invalid in regions which contain highly absorbing materials (such as control rods) or near interfaces between regions having different scattering properties (such as near reflectors). In a highly heterogeneous reactor, these problems are augmented by the fact that a large number of regions are required for accurate presentation of the reactor geometry.

A standard way to overcome this difficulty (Henry, 1975) is to introduce a set of "homogenized" nuclear parameters that replace those of the different materials making up regions in the "real" heterogeneous node. This new set of "homogenized" parameters is evaluated on the basis that it correctly reproduces the interaction rates in an integral sense over those heterogeneous regions of the node under consideration. Consequently, a heterogeneous reactor can be transformed into one that consists of relatively large homogeneous nodes resulting in considerable reduction in computational costs (provided we manage to get these new sets of "homogenized" nuclear parameters). Having achieved that goal, a nodal method can be used to predict accurately the over-all core behavior.

Failure to reproduce exact results using standard homogenization techniques (such as flux weighting) prompted Smith (Smith, 1980) to develop an alternative method. This procedure was a variant of that suggested by Koebke (Koebke, 1979). In this method, Smith introduced correction factors, known as "discontinuity factors", to correct for errors associated with homogenization techniques. These parameters, when used in a nodal scheme, reproduce reference results.

1.2.2. Nodal Diffusion Methods

The essence of nodal methods is the reduction of computational costs through reduction of the number of nodes needed to represent the reactor accurately. For the same accuracy level, nodal methods typically reduced the execution time required to solve a given problem by two orders of magnitude over the finite-difference counterpart.

The first step in deriving a nodal method (common to all schemes) is to derive the nodal balance equation by integrating the Boltzman transport equation over all directions of neutron travel, over individual energy groups and over the volume of a node. To solve the nodal balance equation coupling relations that relate the volume-averaged flux and the face-averaged currents are needed. Fick's Law is used to obtain the desired relation. However, using Fick's Law in conjunction with a finite difference or any higher order approximation introduces additional unknowns to the problem namely, the face-averaged fluxes. A second coupling relation is therefore required to solve the problem.

Early nodal methods (Delp et al., 1964) generally used empirical coupling parameters which were determined from the results of detailed fine-mesh calculations or from actual operating data. More recent nodal schemes have used coupling equations found by integrating the group diffusion equations for the node over transverse directions. To solve the resultant "coupling equation" the transverse-integrated flux is often assumed to be a polynomial (Cadwell, 1967, Finnemann and Wagner, 1975 and Zerkle, 1992) (hence the name polynomial nodal method). One of the principal advantages of polynomial nodal methods is that they have no restriction on the number of energy groups that are to be modeled.

Another approach to solving the transverse-integrated diffusion equation is to do so analytically. This gives rise to the Analytic Nodal Method developed at MIT by Smith (Smith, 1979). This method, incorporated in the computer code QUANDRY, has demonstrated that very accurate

solutions can be obtained with assembly-sized spatial meshes. The computational efficiency of the method has been shown to be at least two orders of magnitude greater than that of finite-difference methods. However, because of its complexity, the analytical nodal method is effectively restricted to modeling problems with no more than two energy groups.

As stated before, nuclear reactors having hexagonal geometry have become more attractive for a wide range of applications in the nuclear industry. One of these applications is the production of special isotopes in the heavy water moderated reactors at the Savannah River Site, usually known as "K-reactors". They are heavy water moderated and cooled, low pressure and low temperature reactors used for plutonium and/or tritium production. Figure (1.1) gives an overview of a typical cross sectional area of one of those reactors.

The success of nodal methods in Cartesian-geometry systems has prompted the development of analogous techniques for systems having hexagonal geometry. The Analytic Nodal Method was applied to hexagonal-shaped nodes by Yarman (Yarman, 1983), but resulted in limited accuracy. Other hexagonal nodal techniques have been developed and successfully applied to fast reactors (Lawrence, 1983, and Wagner, 1989). Also, a finite-difference nodal model (Gehin, 1990) was used to analyze small reflected reactors composed of Savannah River type fuel assemblies for which heterogeneity and mesh effects were corrected by the use of discontinuity factors. It turned out that discontinuity factors found from a infinite lattice calculations led to a unacceptably large errors for the finite reactor case. Moreover, errors were about the same even if the hexagonal cells for those

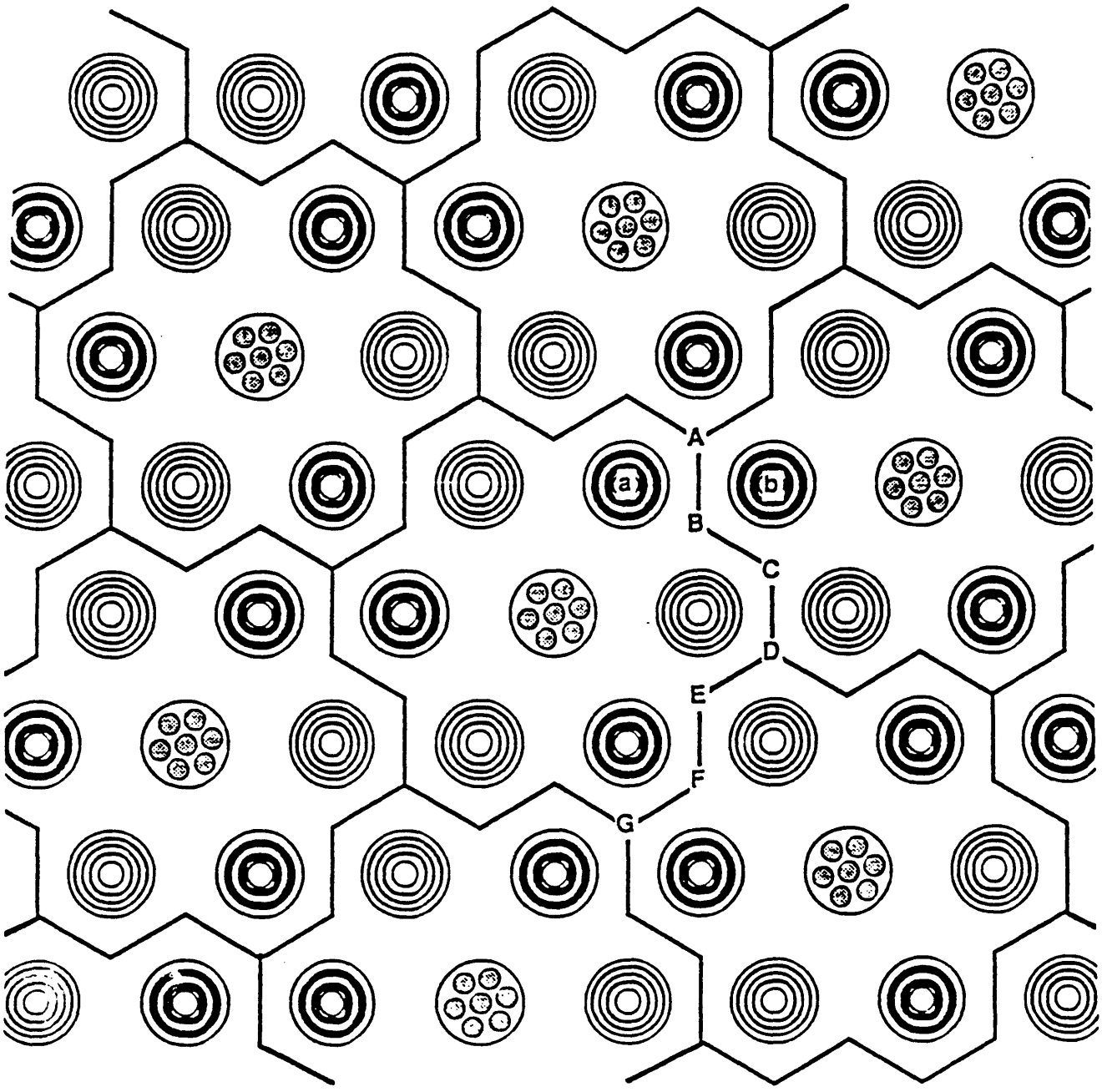

Figure (1.1) An overview of a typical cross sectional area of a "K-reactor".

infinite calculations were homogeneous. Finally, there is an ongoing effort (Taiwo and Khalil, 1991 and 1992) to add a nodal kinetics capability to the ANL DIF3D (Lawrence, 1983) code where the nodal hex-z spatial differencing technique and the theta method for time integration are used.

1.3 Objective of the Present Research

The objective of the present research is to develop and implement a method for analyzing three-dimensional static and transient behavior of reactors composed of regular hexagonal subregions in radial planes. The intent is to develop a nodal code in hex-z geometry capable of solving few-group diffusion equations that predict the static as well as the transient behavior of node-averaged group-fluxes. To correct for errors due to nodal-homogenization and the use of the diffusion theory model, discontinuity factors will be used, and a procedure for finding them by editing a lattice spectrum will be worked out. Also, the assumption that transverse-integrated group fluxes have quadratic (rather than flat) shapes across a hex will be incorporated. This latter model should yield much more accurate results and, when it is used, the discontinuity factors will be correcting primarily for the heterogeneous nature of the nodes, rather than for both heterogeneity and mesh size effects. This report describes a code that has been written to implement the above method and to incorporate a simple, constant pressure, one-dimensional (parallel channel) thermal-hydraulic model has been written.

1.4 Thesis Structure

In Chapter (2) the static, three-dimensional, few-group nodal equations are derived. First, the Boltzman equation is integrated over all directions and over an energy range. The result is integrated over a node yielding a nodal balance equation. Next, Fick's law is introduced along with the quadratic-shape approximation for the transverse-integrated fluxes creating a set of linear algebraic equations which are then solved for the volume-averaged group fluxes in each node and the eigenvalue of the system. A method for evaluating the discontinuity factors correcting for errors due to heterogeneity, Fick's law approximation, and quadratic-shape approximation will be outlined. Finally, a simple one-dimensional thermal-hydraulic feedback model will be described.

In Chapter (3) the numerical solution method for solving the eigenvalue problem and for determining the discontinuity factors and newly updated macroscopic cross sections, due to thermal feedback, will be presented, and numerical applications will be discussed.

Chapter (4) is analogous to chapter (2) except for the fact that it will deal with the transient part of the problem. The time dependent Boltzman equation will be transformed to few-group diffusion equations, in a way similar to what is described in Chapter (2). These will be solved for the volume-averaged fluxes for different energy groups at each time step. Also, a simple one-dimensional transient thermal-hydraulic feedback model will be outlined.

In Chapter (5), as in chapter (3), numerical solution methods for the time dependent few-group diffusion equation will be described and numerical applications of the method with and without thermal feedback will be given.

Conclusions of this thesis and recommendations for future work will be presented in Chapter (6).

CHAPTER TWO

SOLUTION OF THE STATIC NEUTRON DIFFUSION EQUATION

2.1 Introduction

The goal of this chapter is to derive the static, three-dimensional (hex-z), few-group nodal diffusion equations with thermal-hydraulic feedback option. For the sake of simplicity, a two-dimensional model will be discussed first, then it will be extended to obtain three-dimensional results. Also, a separate two-dimensional, few-group, finite-difference nodal diffusion model for triangular-shaped nodes will be outlined. The triangular-shaped nodes are required for the calculation of discontinuity factors and for obtaining a fine-mesh, finite difference solution to serve as a reference. Moreover, we shall allow for a general number of energy groups and for upscattering in thermal groups. Finally, a simple, constant pressure, one-dimensional (parallel channel) thermal-hydraulic model will be incorporated.

We begin the derivation by integrating the Boltzman transport equation over all directions to obtain an equation that relates the scalar flux density to the net current density. The resultant equation is then integrated over an energy range and over the volume of the node. The resulting

equation is called a few-group nodal balance equation which is basically a relation between the volume-averaged flux for a node and the face-averaged-currents for that node. To solve the nodal balance equation coupling relations that relate the volume-averaged flux and the face-averaged currents are needed. Fick's Law is used to obtain the desired relation. However, using Fick's Law in conjunction with a finite difference or any higher order approximation introduces additional unknowns to the problem namely, the face-averaged fluxes. Up to this point there is no distinction between the hexagonal- and the triangular-shaped-node models mentioned above, but this similarity will cease to exist when each model introduces the second coupling equation needed to solve the nodal balance equation. In the triangular-shaped-node model the face-averaged fluxes are assumed to have a flat shape across the node, whereas in the hexagonal-shaped-node model they are assumed to have a quadratic one. Discontinuity factors edited from the fine-mesh, finite difference, triangular-shaped-node model will be used in the hexagonal model to correct for mesh size effects, the Fick's Law approximation and homogenization effects (if applicable).

Finally, a steady state WIGL (Vota, 1969) thermal-hydraulic model is incorporated as a feedback mechanism to update the nuclear cross sections. Average fuel and coolant temperatures and average coolant density are calculated for each node based on the power level of the system. These three variables are used to update the nuclear parameters of the core by linear interpolation.

2.2 Derivation of the Nodal Equations

By integrating the Boltzman neutron transport equation over all directions and over an energy group g it is possible to obtain formally (Henry, 1975)

$$\nabla.\underline{J}_g(\underline{r}) + \Sigma_g(\underline{r})\phi_g(\underline{r}) = \sum_{g'=1}^{G} \frac{1}{\lambda}\chi_g \nu\Sigma_{fg'}(\underline{r})\phi_{g'}(\underline{r}) + \sum_{\substack{g'=1 \\ g'\neq g}}^{G} \Sigma_{gg'}(\underline{r})\phi_{g'}(\underline{r}); \quad g = 1,2,....,G \tag{2.1}$$

where

G ≡ total number of energy groups,

$\phi_g(\underline{r})$ ≡ group g scalar flux density,

$\underline{J}_g(\underline{r})$ ≡ group g net current density,

$\Sigma_g(\underline{r})$ ≡ group g total macroscopic cross section minus the group g in-group scattering cross section,

λ ≡ the critical eigenvalue (K_{eff}),

χ_g ≡ neutron fission spectrum for group g,

$\nu\Sigma_{fg}(\underline{r})$ ≡ number of neutrons emitted per fission multiplied by the macroscopic fission cross section for group g,

$\Sigma_{gg'}(\underline{r})$ ≡ macroscopic scattering cross section from group g' to group g.

Next, we integrate Equation (2.1) over the area of an arbitrary node-l to obtain

$$\frac{s}{A}\sum_{p=1}^{P} \bar{J}^l_{gp} + \bar{\bar{\Sigma}}^l_g \bar{\bar{\varphi}}^l_g = \frac{1}{\lambda}\sum_{g'=1}^{G} \chi_g \bar{\bar{\nu\Sigma}}^l_{fg'} \bar{\bar{\varphi}}^l_{g'} + \sum_{\substack{g'=1 \\ g'\neq g}}^{G} \bar{\bar{\Sigma}}^l_{gg'} \bar{\bar{\varphi}}^l_{g'} \tag{2.2}$$

where

s ≡ node face length,

A ≡ node area,

l ≡ index representing the node upon which the balance is performed,

p ≡ an index representing the faces of a node;

p = 1,2,....,P; P being the number of faces (node faces orientation is shown in Figure (2.1) for both triangular and hexagonal models), and

$$\bar{J}^{l}_{gp} \equiv \frac{1}{s}\int_{s_p} \underline{J}_g(\underline{r})\cdot\underline{n}_p ds;\ p = 1,2,...,P$$

$$\bar{\bar{\varphi}}^{l}_{g} \equiv \frac{1}{A}\int_{A} \phi_g(\underline{r})dA,$$

$$\bar{\bar{\Sigma}}^{l}_{g}\bar{\bar{\varphi}}^{l}_{g} \equiv \frac{1}{A}\int_{A} \Sigma_g(\underline{r})\phi_g(\underline{r})dA, \qquad (2.3)$$

$$\bar{\nu\Sigma}^{l}_{fg}\bar{\bar{\varphi}}^{l}_{g} \equiv \frac{1}{A}\int_{A} \nu\Sigma_{fg}(\underline{r})\phi_g(\underline{r})dA,$$

$$\bar{\Sigma}^{l}_{gg'}\bar{\bar{\varphi}}^{l}_{g'} \equiv \frac{1}{A}\int_{A} \Sigma_{gg'}(\underline{r})\phi_{g'}(\underline{r})dA.$$

Note that (for the two-dimensional case) we have assumed that all nodes have the same area, that the node spacing is constant, and that all nodes have regular geometry so that the face length is the same for all faces. Also, note that according to the definition given above, $\bar{J}^{l}_{gp}$ is the face-averaged

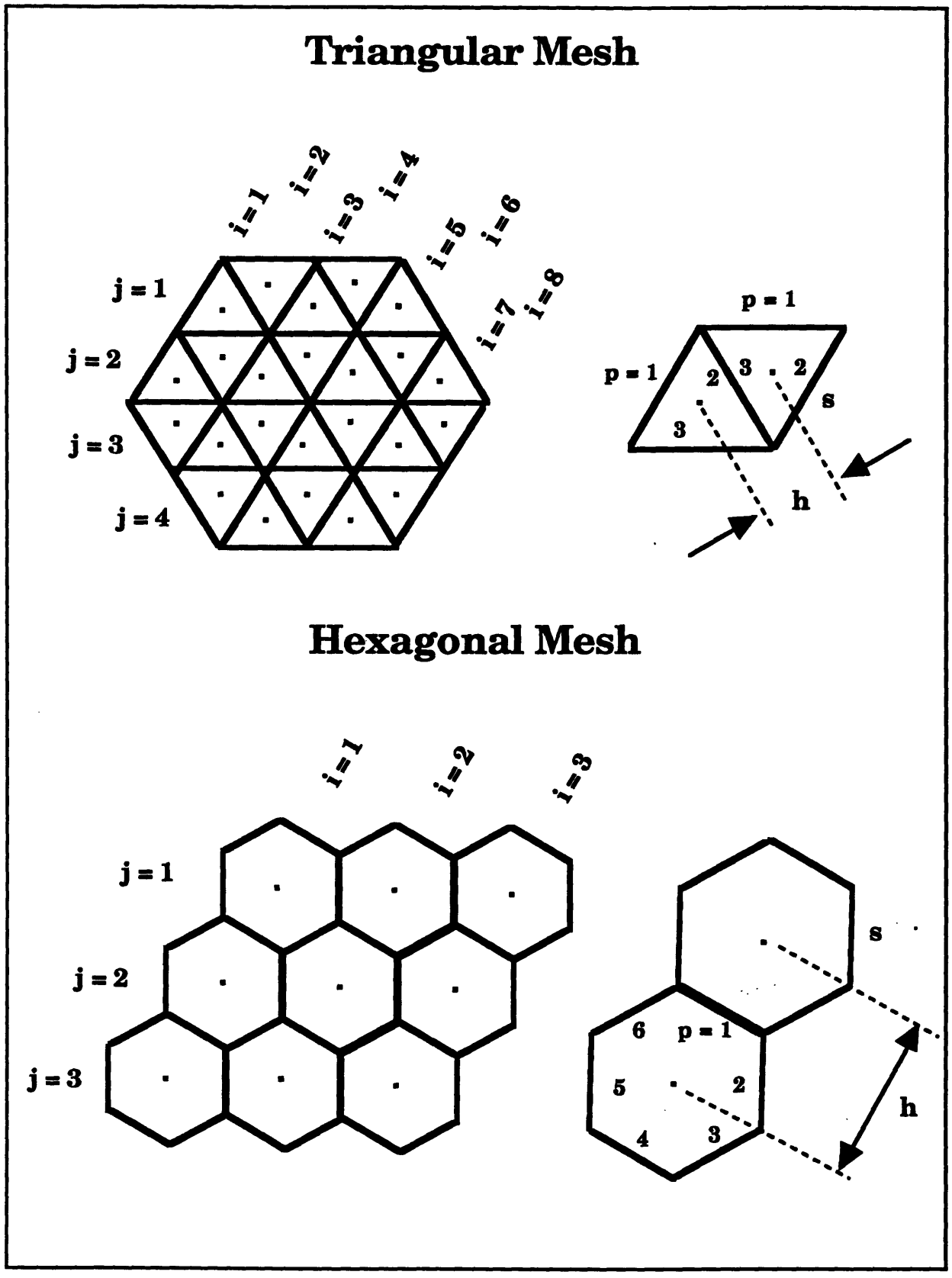

Figure (2.1) Examples of the notation used in the derivation of the nodal equations

current leaving node-l through face p which has an outward-directed normal unit vector $\underline{n}_p$.

As stated before, the objective here is to solve the nodal balance equation for the volume-averaged fluxes, $\bar{\bar{\varphi}}^l_g$, and the system eigenvalue, λ. But as it is obvious from Equation (2.2) we need another relationship between the face-averaged currents and the volume-averaged flux to be able to reach our goal. This can be attained by using Fick's Law

$$\underline{J}(\underline{r},E) \approx -D(\underline{r},E)\, \nabla\phi(\underline{r},E). \qquad (2.4)$$

This approximation, as will be clear in the coming two sections, introduces additional unknowns (the face-averaged fluxes) to the problem, and the way we are going to deal with those new unknowns in the triangular-shaped-node model will be different from the way we deal with them in the hexagonal one.

2.2.1 Triangular-Shaped-Node Model

In this model, Equation (2.4) is cast into energy group form and integrated over node-l assuming the flux divergence to have a truncation error of the first order, O(h), i.e. "finite difference approximation". This will allow us to write the face-averaged current in the form

$$\bar{J}^l_{gp} \approx -\bar{D}^l_g \frac{\bar{\varphi}^l_{gp} - \bar{\bar{\varphi}}^l_g}{h/2}. \qquad (2.5)$$

In this equation $\overline{D}_g^l$ is the homogenized diffusion constant for node-l and $\overline{\varphi}_{gp}^l$ is the group flux, averaged over face p of node-l (the face-averaged flux) given by

$$\overline{\varphi}_{gp}^l \equiv \frac{1}{s}\int_{s_p} \phi_g(\underline{r})ds. \qquad (2.6)$$

Similarly for node-m, adjacent to node-l at face-p, we can write

$$\overline{J}_{gp}^m \approx - \overline{D}_g^m \frac{\overline{\varphi}_{gp}^m - \overline{\overline{\varphi}}_g^m}{h/2}. \qquad (2.7)$$

We know that the net current and the flux densities must be continuous across the interface between nodes l and m so that

$$\overline{J}_{gp}^l = - \overline{J}_{gp}^m \qquad (2.8)$$

and

$$\overline{\varphi}_{gp}^l = \overline{\varphi}_{gp}^m. \qquad (2.9)$$

Equations (2.5) and (2.7) are good approximations provided that diffusion theory is valid, the nodes are truly homogeneous (or there is no ambiguity in finding homogenized diffusion constants), and the mesh spacing is small. If this is the case, we can combine these two relations (using the continuity conditions (2.8) and (2.9)) and eliminate the face-averaged flux. Substituting the resulting relation for $\overline{J}_{gp}^l$ into Equation (2.2) gives a standard form of finite-difference equations

$$\frac{2s}{A}\sum_{p=1}^{3}\left[\frac{1}{\overline{D}_g^l}+\frac{1}{\overline{D}_g^m}\right]^{-1}\left[\bar{\bar{\varphi}}_g^l-\bar{\bar{\varphi}}_g^m\right]+\bar{\Sigma}_g^l\bar{\bar{\varphi}}_g^l$$

$$=\frac{1}{\lambda}\sum_{g'=1}^{G}\chi_g\overline{\nu\Sigma}_{fg'}^l\bar{\bar{\varphi}}_{g'}^l+\sum_{\substack{g'=1\\g'\neq g}}^{G}\bar{\Sigma}_{gg'}^l\bar{\bar{\varphi}}_{g'}^l \qquad (2.10)$$

$$g = 1, 2, ..., G$$

which can be solved for the volume-averaged flux $\bar{\bar{\varphi}}_g^l$.

The reason for solving the nodal balance equation for the triangular geometry is twofold: the solution will serve as 1) a reference, and 2) a means for determining the discontinuity factors for the hexagonal geometry.

2.2.2 Hexagonal-Shaped-Node Model

The essential approximations of the hexagonal model are best described by referring to Figure (2.2), which shows two neighboring hexagonal nodes, for which it is assumed that homogenized group-diffusion theory parameters are available. (The nodes might, in physical fact, be heterogeneous with a pitch (h) of ~ 18 cm.) Also, we shall drop the energy group index from now on for the sake of simplicity with the understanding that all results obtained are for any energy-group g. From the figure we can define the transverse integrated flux for the x-direction as

$$\bar{\varphi}^{ij}(x)\equiv\frac{1}{s+\frac{2}{\sqrt{3}}(x-x_i)}\int_{-\frac{s}{2}-\frac{x-x_i}{\sqrt{3}}}^{\frac{s}{2}+\frac{x-x_i}{\sqrt{3}}}\phi(x,y)\,dy \quad ; \; x_i\le x\le x_i+\frac{h}{2}$$

$$\equiv\frac{1}{s+\frac{2}{\sqrt{3}}(x_{i+1}-x)}\int_{-\frac{s}{2}-\frac{x_{i+1}-x}{\sqrt{3}}}^{\frac{s}{2}+\frac{x_{i+1}-x}{\sqrt{3}}}\phi(x,y)\,dy \quad ; \; x_i+\frac{h}{2}\le x\le x_{i+1} \qquad (2.11)$$

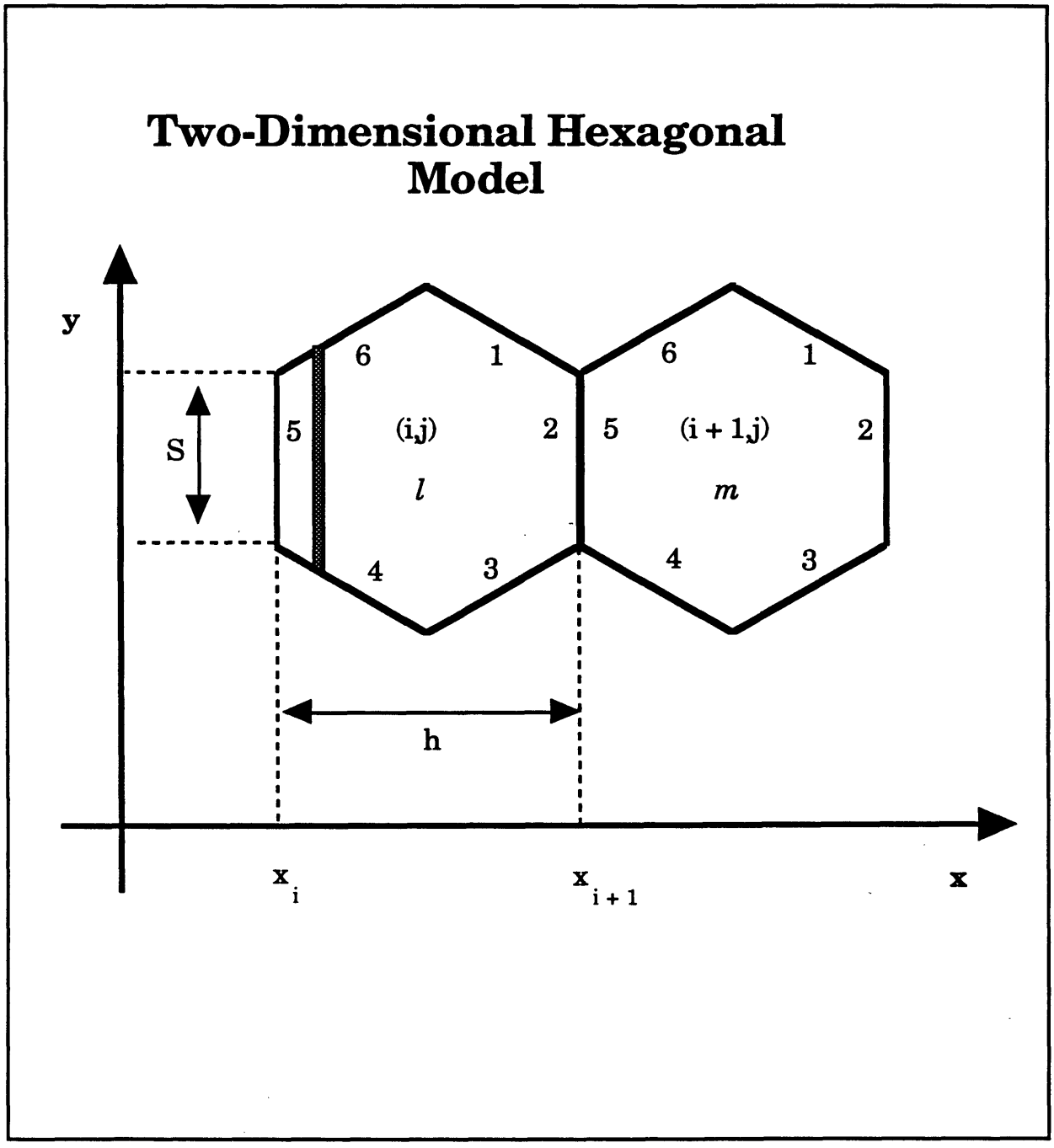

Figure (2.2) Two neighboring hexagonal nodes

Note that if $\phi(x,y)$ is a constant, C, then $\bar{\varphi}^{ij}(x)$ also equals C. For $\phi(x,y)$ = C, the integrals in Equation (2.11) form a tent-like function of x. To obtain an improved nodal coupling equation when $\phi(x,y)$ is not flat, we approximate the shape of $\bar{\varphi}^{ij}(x)$ in the range (x_i, x_{i+1}) as a quadratic in x.(Shatilla and Henry, 1992)

$$\bar{\varphi}^{ij}(x) = \bar{\varphi}^{ij}(x_i)[1-4v+3v^2] + \bar{\varphi}^{ij}(x_{i+1})[-2v+3v^2] + \left\{\frac{12}{13}\bar{\bar{\varphi}}^{ij} + \frac{1}{26}\left(\bar{\varphi}^{ij}(x_{i+1}) + \bar{\varphi}^{ij}(x_i)\right)\right\}6[v-v^2] \quad ; \quad v\ (\equiv \frac{x-x_i}{h}) \tag{2.12}$$

where the three quadratics in v have been chosen so that $\bar{\varphi}^{ij}(x_i)$, $\bar{\varphi}^{ij}(x_{i+1})$ and $\bar{\bar{\varphi}}^{ij}$ appear as coefficients.

For the range $x_i \le x \le x_i + h/2$, multiplying Equation (2.11) by $(s + 2(x - x)/\sqrt{3})$ and differentiating both sides (using for the right hand side the rule for differentiating a definite integral), and evaluating the result at $x = x_i$ yields

$$\frac{2}{\sqrt{3}}\bar{\varphi}^{ij}(x_i) + s\left\{-\frac{49}{13h}\bar{\varphi}^{ij}(x_i) - \frac{23}{13h}\bar{\varphi}^{ij}(x_{i+1}) + \frac{72}{13h}\bar{\bar{\varphi}}^{ij}\right\} = \frac{1}{\sqrt{3}}\left[\phi(x_i,\frac{s}{2}) + \phi(x_i,-\frac{s}{2})\right] - \int_{-\frac{s}{2}}^{+\frac{s}{2}} \frac{J_x(x_i,y)}{\bar{D}^{ij}}dy \tag{2.13}$$

provided that we use the diffusion theory approximation

$$J_x(x,y) = -\bar{D}^{ij}\frac{\partial\phi(x,y)}{\partial x} \tag{2.14}$$

(where $\bar{D}^{ij}$ is the homogenized diffusion coefficient for node (i,j)).

If, in keeping with the convention that the surface-averaged net currents are all directed out of the hexagon (i,j), we define

$$J_5^{ij} \equiv -\frac{1}{s}\int_{-\frac{s}{2}}^{+\frac{s}{2}} J_x(x_i,y)dy \qquad (2.15)$$

and make the assumption that

$$\varphi^{ij}(x_i) = \frac{1}{2}\left\{\phi(x_i, \frac{s}{2}) + \phi(x_i, -\frac{s}{2})\right\} \qquad (2.16)$$

Equation (2.13) simplifies to

$$J_5^{ij} = -\frac{\overline{D}^{ij}}{h}\left\{\frac{49}{13}\bar{\varphi}_5^{ij} - \frac{72}{13}\bar{\bar{\varphi}}^{ij} + \frac{23}{13}\bar{\varphi}_2^{ij}\right\} \qquad (2.17)$$

where

$$\begin{aligned} \bar{\varphi}_2^{ij} &\equiv \bar{\varphi}^{ij}(x_{i+1}) \\ \bar{\varphi}_5^{ij} &\equiv \bar{\varphi}^{ij}(x_i) \end{aligned} \qquad (2.18)$$

Since it is based on a quadratic expansion of the transverse integrated flux, Equation (2.17) should be more accurate than one based on the finite-difference approximation. However, it contains average surface fluxes on two node faces, and both of these will have to be eliminated if we are to express J_5^{ij} in terms only of volume-averaged fluxes such as $\bar{\bar{\varphi}}^{ij}$. To do this we first apply to the other half of the node $x_i + h/2 \le x \le x_{i+1}$ a procedure analogous to that just described. The result is

$$J_2^{ij} = -\frac{\bar{D}^{ij}}{h}\left\{\frac{23}{13}\bar{\varphi}_5^{ij} - \frac{72}{13}\bar{\bar{\varphi}}^{ij} + \frac{49}{13}\bar{\varphi}_2^{ij}\right\} \qquad (2.19)$$

By manipulating Equations (2.17) and (2,19) we obtain

$$J_2^{ij} - \frac{49}{23}J_5^{ij} = -\frac{\bar{D}^{ij}}{h}\left\{-\frac{144}{23}\bar{\varphi}_5^{ij} + \frac{144}{23}\bar{\bar{\varphi}}^{ij}\right\} \qquad (2.20)$$

and

$$\frac{49}{23}J_2^{ij} - J_5^{ij} = -\frac{\bar{D}^{ij}}{h}\left\{+\frac{144}{23}\bar{\varphi}_2^{ij} - \frac{144}{23}\bar{\bar{\varphi}}^{ij}\right\} \qquad (2.21)$$

Since $\bar{\varphi}_2^{ij} = \bar{\varphi}_5^{i+1,j}$ and $J_5^{ij} = J_2^{i+1,j}$ (see Figure (2.2)), it is tempting to rewrite Equation (2.20) for $i \rightarrow i+1$ and eliminate $\bar{\varphi}_2^{ij}$ from the result thereby obtaining an equation relating J_5^{ij}, J_2^{ij} and $J_2^{i+1,j}$ to $\bar{\bar{\varphi}}^{ij}$ and $\bar{\bar{\varphi}}^{i+1,j}$. This result, along with analogous equations for the faces (3,6) and (4,1) combined with nodal balance Equation (2.2) form a set of equations that can be solved for the volume-averaged fluxes and face-averaged currents. Unfortunately, no efficient iterative procedure has been found for solving the resultant equations. Accordingly, we have taken a different approach motivated by the fact that for small mesh intervals, h, the resultant equations will take on the finite-difference form for which there are well known, efficient iterative solution procedures.

To attain this goal we add the nodal Equation (2.2) to Equation (2.21) (after reintroducing the energy group index g and after taking note of the fact that the node (i,j) is the same as node-l) to obtain

$$\frac{72}{23}\bar{J}^{l}_{g2} + \sum_{p\neq 2,5}\bar{J}^{l}_{gp} + \frac{3h}{2}\bar{\Sigma}^{l}_{g}\bar{\bar{\varphi}}^{l}_{g} = \frac{3h}{2\lambda}\sum_{g'=1}^{G}\chi_g\overline{\nu\Sigma}^{l}_{fg'}\bar{\bar{\varphi}}^{l}_{g'} + \sum_{\substack{g'=1\\ g'\neq g}}^{G}\frac{3h}{2}\bar{\Sigma}^{l}_{gg'}\bar{\bar{\varphi}}^{l}_{g'} - \frac{\bar{D}^{l}_{g}}{h}\left\{+\frac{144}{23}\bar{\varphi}^{l}_{g2} - \frac{144}{23}\bar{\bar{\varphi}}^{l}_{g}\right\} \tag{2.22}$$

Then we subtract Equation (2.2) from Equation (2.20), but write the result with i replaced by i + 1 (node-l replaced by node-m)

$$-\frac{72}{23}\bar{J}^{m}_{g5} - \sum_{p\neq 2,5}\bar{J}^{m}_{gp} - \frac{3h}{2}\bar{\Sigma}^{m}_{g}\bar{\bar{\varphi}}^{m}_{g} = -\frac{3h}{2\lambda}\sum_{g'=1}^{G}\chi_g\overline{\nu\Sigma}^{m}_{fg'}\bar{\bar{\varphi}}^{m}_{g'} - \sum_{\substack{g'=1\\ g'\neq g}}^{G}\frac{3h}{2}\bar{\Sigma}^{m}_{gg'}\bar{\bar{\varphi}}^{m}_{g'} - \frac{\bar{D}^{m}_{g}}{h}\left\{-\frac{144}{23}\bar{\varphi}^{m}_{g5} + \frac{144}{23}\bar{\bar{\varphi}}^{m}_{g}\right\} \tag{2.23}$$

Since $\bar{\varphi}^{l}_{g2} = \bar{\varphi}^{m}_{g5}$ and $\bar{J}^{l}_{g2} = -\bar{J}^{m}_{g5}$ we can multiply Equation (2.22) by $1/\bar{D}^{l}_{g}$ and add it to Equation (2.23) multiplied by $1/\bar{D}^{m}_{g}$ and thereby eliminate the surface-averaged fluxes obtaining $\bar{J}^{l}_{g2}$ in terms of $\bar{\varphi}^{l}_{g2}$, $\bar{\bar{\varphi}}^{m}_{g}$ and 8 transverse currents.

However, before doing so we force Equations (2.22) and (2.23) to be exact by introducing "discontinuity factors". Specifically, to take care of the fact that the nodes are really heterogeneous, that diffusion theory may not be valid, that $\varphi^{ij}(x_i)$ may be approximated by Equation (2.16), and that the quadratic expansion of the flux may still be inaccurate, we multiply $\bar{\varphi}^{l}_{g2}$ in Equation (2.22) by $1/f^{l}_{g2}$. Similarly, we multiply $\bar{\varphi}^{m}_{g5}$ in Equation (2.23) by $1/f^{m}_{g5}$ to force the two results to be exact. Then we eliminate $\bar{\varphi}^{l}_{g2}$ and $\bar{\varphi}^{m}_{g5}$. The result is

$$\bar{J}^{l}_{g2} = -\bar{J}^{m}_{g5} = \{\frac{h}{2}[\frac{f^{m}_{g5}}{\bar{D}^{m}_{g}} + \frac{f^{l}_{g2}}{\bar{D}^{l}_{g}}]\}^{-1}\{\sum_{p\neq 2,5}^{6}\frac{23h}{144}[\bar{J}^{l}_{gp}\frac{f^{l}_{g2}}{\bar{D}^{l}_{g}} - \bar{J}^{m}_{gp}\frac{f^{m}_{g5}}{\bar{D}^{m}_{g}}]$$
$$+ f^{m}_{g5}\{1 - \frac{23h^{2}}{96\bar{D}^{m}_{g}}[\bar{\Sigma}^{m}_{g}\bar{\bar{\varphi}}^{m}_{g} - \frac{1}{\lambda}\sum_{g'=1}^{G}\chi_{g}\bar{\nu\Sigma}^{m}_{fg'}\bar{\bar{\varphi}}^{m}_{g'} - \sum_{\substack{g'=1\\g'\neq g}}^{G}\bar{\Sigma}^{m}_{gg'}\bar{\bar{\varphi}}^{m}_{g'}]\} \qquad (2.24)$$
$$- f^{l}_{g2}\{1 - \frac{23h^{2}}{96\bar{D}^{l}_{g}}[\bar{\Sigma}^{l}_{g}\bar{\bar{\varphi}}^{l}_{g} - \frac{1}{\lambda}\sum_{g'=1}^{G}\chi_{g}\bar{\nu\Sigma}^{l}_{fg'}\bar{\bar{\varphi}}^{l}_{g'} - \sum_{\substack{g'=1\\g'\neq g}}^{G}\bar{\Sigma}^{l}_{gg'}\bar{\bar{\varphi}}^{l}_{g'}]\}\}$$

Substituting this result (along with the analogous expression for the other five currents across the faces of the hexagon) into the nodal balance Equation (2.2) yields an equation coupling the volume-averaged flux in node-l to the volume-averaged fluxes in its six neighbors (m = 1, 2,..., 6). Transverse face-current terms (the summation over p in Equation (2.24) will appear in this "seven-point" nodal equation. These must be updated iteratively using Equation (2.24) and the analogous equations for the other five currents across the node faces.

Finally, if we consider the derivation of Equation (2.24) we find that the net effect of the introduction of the discontinuity factors is allow two fictitious face-averaged fluxes to be discontinuous across the interface. Thus, we define fictitious face-averaged fluxes $\bar{\varphi}^{l\,(\mathrm{hom})}_{gp}$ and $\bar{\varphi}^{m\,(\mathrm{hom})}_{gp}$ as

$$\bar{\varphi}^{l\,(\mathrm{hom})}_{gp} \equiv \frac{\bar{\varphi}^{l}_{gp}}{f^{l}_{gp}}$$

and

$$\bar{\varphi}^{m\,(\mathrm{hom})}_{gp} \equiv \frac{\bar{\varphi}^{m}_{gp}}{f^{m}_{gp}}$$

Since the physical face-averaged fluxes $\bar{\varphi}^{l}_{gp}$ and $\bar{\varphi}^{m}_{gp}$ are continuous across the interface, the continuity condition that is implied for $\bar{\varphi}^{l\,(hom)}_{gp}$ and $\bar{\varphi}^{m\,(hom)}_{gp}$ across the boundary between nodes l and m is

$$\bar{\varphi}^{l(hom)}_{gp}\, f^{l}_{gp} = \bar{\varphi}^{m\,(hom)}_{gp}\, f^{m}_{gp}$$

Since the correction factors f^{l}_{gp} and f^{m}_{gp} are generally not equal, the above equality indicates that the fictitious surface fluxes must be discontinuous; hence the name discontinuity factors.

2.2.3 Evaluation of Discontinuity Factors

The above model will not be complete until we outline a procedure by which the discontinuity factors introduced into Equation (2.24) can be evaluated.

Rewriting Equations (2.22) and (2.23) with discontinuity factors inserted yields

$$\frac{72}{23}\bar{J}^{l}_{g2} + \sum_{p\neq 2,5} \bar{J}^{l}_{gp} + \bar{\bar{\Sigma}}^{l}_{g}\bar{\bar{\varphi}}^{l}_{g} = \frac{1}{\lambda}\sum_{g'=1}^{G} \chi_g \bar{\bar{\nu\Sigma}}^{l}_{fg'}\bar{\bar{\varphi}}^{l}_{g'} + \sum_{\substack{g'=1\\ g'\neq g}}^{G} \bar{\bar{\Sigma}}^{l}_{gg'}\bar{\bar{\varphi}}^{l}_{g'} - \frac{\bar{D}^{l}_{g}}{h}\left(+\frac{144\,\bar{\varphi}^{l}_{g2}}{23\, f^{l}_{g2}} - \frac{144}{23}\bar{\bar{\varphi}}^{l}_{g}\right) \tag{2.25}$$

and

$$-\frac{72}{23}\bar{J}^{m}_{g5} - \sum_{p\neq 2,5} \bar{J}^{m}_{gp} - \bar{\bar{\Sigma}}^{m}_{g}\bar{\bar{\varphi}}^{m}_{g} = -\frac{1}{\lambda}\sum_{g'=1}^{G} \chi_g \bar{\bar{\nu\Sigma}}^{m}_{fg'}\bar{\bar{\varphi}}^{m}_{g'} - \sum_{\substack{g'=1\\ g'\neq g}}^{G} \bar{\bar{\Sigma}}^{m}_{gg'}\bar{\bar{\varphi}}^{m}_{g'} - \frac{\bar{D}^{m}_{g}}{h}\left(-\frac{144\,\bar{\varphi}^{m}_{g5}}{23\, f^{m}_{g5}} + \frac{144}{23}\bar{\bar{\varphi}}^{m}_{g}\right) \tag{2.26}$$

from which we can get

$$f_{gp}^{l} = \frac{\bar{\varphi}_{gp}^{l}}{\frac{23h}{144\bar{D}_{g}^{l}}\left[-\frac{72}{23}\bar{J}_{gp}^{l} - \sum_{p' \neq 2,5} \bar{J}_{gp'}^{l} - \bar{\Sigma}_{g}^{l}\bar{\bar{\varphi}}_{g}^{l} + \frac{1}{\lambda}\sum_{g'=1}^{G} \chi_{g}\overline{\nu\Sigma}_{fg'}^{l}\bar{\bar{\varphi}}_{g'}^{l} + \sum_{\substack{g'=1 \\ g' \neq g}}^{G} \bar{\Sigma}_{gg'}^{l}\bar{\bar{\varphi}}_{g'}^{l}\right] + \bar{\bar{\varphi}}_{g}^{l}} \tag{2.27a}$$

Another way to determine discontinuity factors is to use Equation (2.20), after inserting the discontinuity factor, to get the following

$$f_{gp}^{l} = \frac{\bar{\varphi}_{gp}^{l}}{\frac{23h}{144\bar{D}_{g}^{l}}\left[-\frac{49}{23}\bar{J}_{gp}^{l} + \bar{J}_{gx}^{l}\right] + \bar{\bar{\varphi}}_{g}^{l}} \text{; where } x = p + 3 \text{ if } p \leq 3 \text{ else } x = p - 3 \tag{2.27b}$$

And similarly, we can get expressions for discontinuity factors for the other five faces of a hexagon provided that we know all the variables on the right hand side of Equation (2.27). One way to achieve that is to do a fine-mesh finite-difference (triangular-shaped-node model) calculations to determine the face-averaged fluxes and currents and the volume-averaged fluxes for all the nodes in the system then edit the discontinuity factors according Equation (2.27). This procedure would be redundant since, if we had already analyzed the whole core, the problem would have been solved and no further calculations would be needed.

A much simpler (but more approximate) approach is to treat identical subregions of the reactor as parts of an infinite lattice for which discontinuity factors can be edited from infinite-lattice, fine-mesh, finite-difference

calculations. For SRS type of reactors, the smallest repeating subregion is shown in Figure (2.3). For infinite-lattice calculations, the arrows indicate the relationship of the net neutron currents. For very simple geometrical structures these infinite-lattice calculations can be performed using the fine triangular mesh shown in Figure (2.4). The dotted region is used to simulate the control, fuel, or target rods and their associated moderator. In practice, the fuel, target, and control regions are not homogeneous so that preliminary homogenization on the cell level is needed to account for heterogeneous, spectral and transport effects. The development of such procedures has not been considered in the present thesis.

Discontinuity factors calculated from Equations (2.27a) and (2.27b) are identical. This suggests that although both equations have different mathematical form and origin, they both carry the same physical information (homogenization, diffusion theory approximation, geometrical effects, and quadratic approximation).

2.3 Boundary Conditions

On each external surface of the system being analyzed boundary conditions must be applied. Boundary conditions of the form

$$\alpha^{l}_{gp}\bar{J}^{l}_{gp} - \beta^{l}_{gp}\bar{\varphi}^{l}_{gp} = 0 \qquad (2.28)$$

will be applied to node-l having an external surface p. All standard boundary conditions can be expressed by the appropriate specification of α^{l}_{gp} and β^{l}_{gp}. Values of α^{l}_{gp} and β^{l}_{gp} for the most common boundary conditions are given in

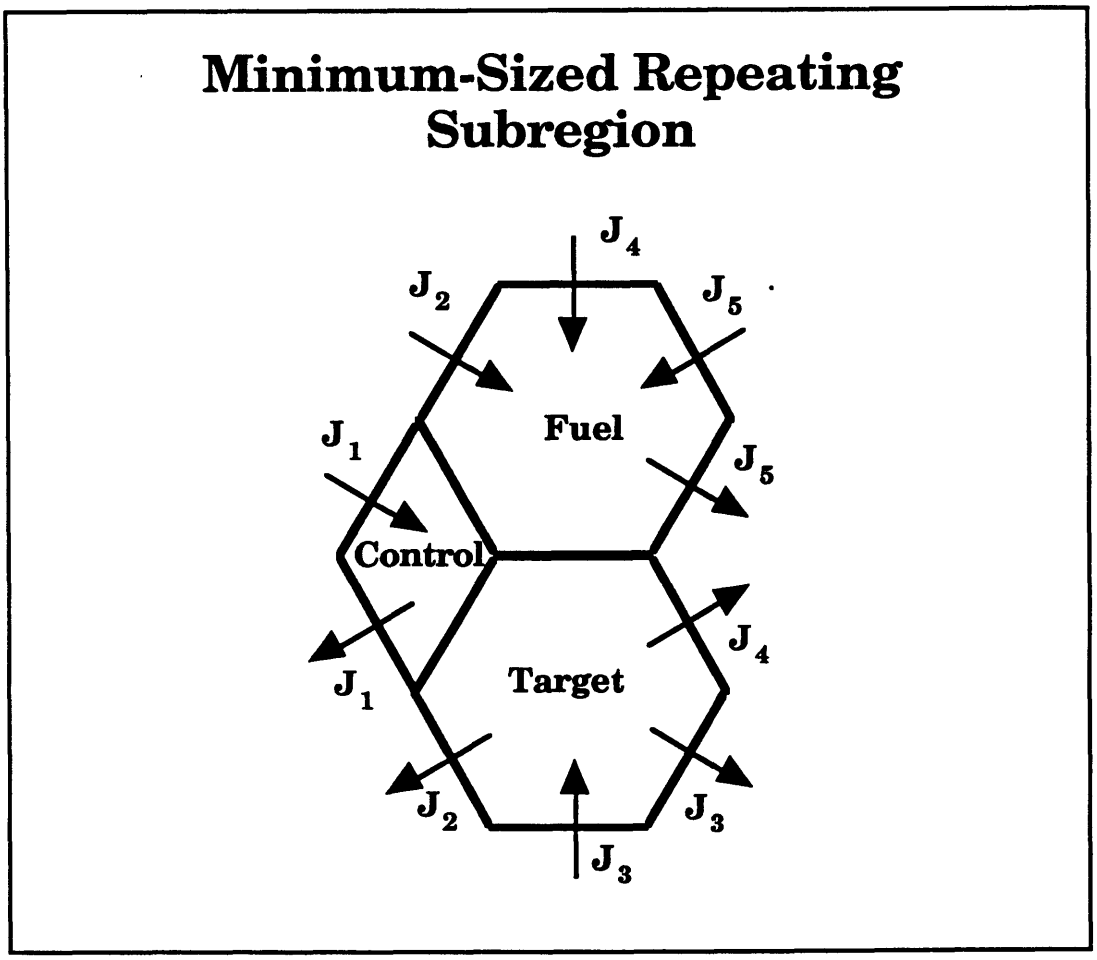

Figure (2.3) Smallest repeating subregion of the SRS reactos. The arrows represent the relationships between currets.

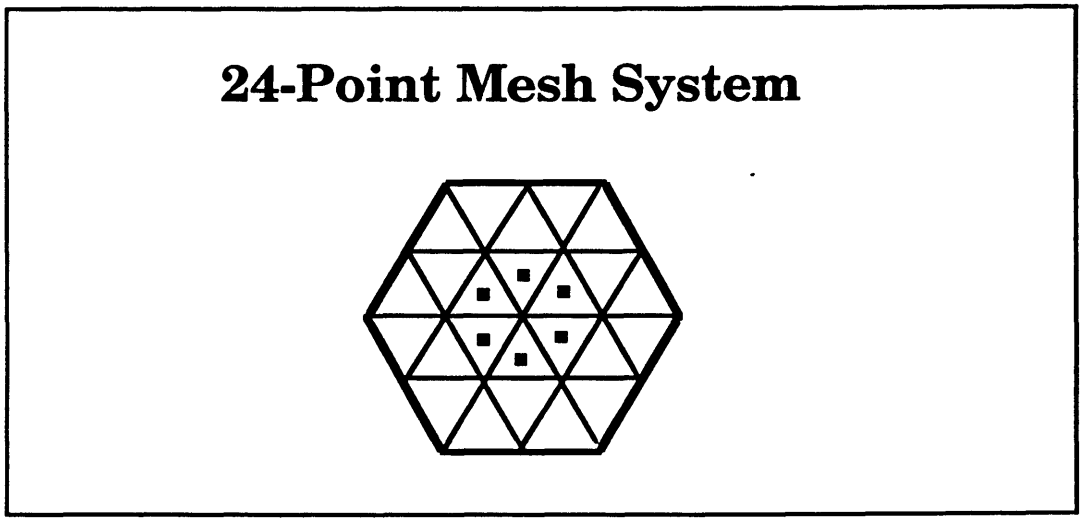

Figure (2.4) Triangular mesh used in reference and infinite-lattice calculations.

Table (2.1).

For external surfaces the following equation replaces Equation (2.24).

$$\bar{J}^l_{gp} = \frac{\dfrac{\beta^l_{gp} f^l_{gp}}{\alpha^l_{gp}}\left[\dfrac{23h\bar{J}^l_{gx}}{144\bar{D}^l_g} + \bar{\bar{\varphi}}^l_g\right]}{1 + \dfrac{49\beta^l_{gp} f^l_{gp} h}{144\alpha^l_{gp}\bar{D}^l_g}} \quad ; \text{ if } p \le 3 \therefore x = p + 3 \quad \text{else} \quad x = p - 3 \qquad (2.29)$$

Table (2.1) Values of α and β for standard boundary conditions.

Boundary Condition	α	β
Zero Flux	0	1
Zero Current	1	0
Zero Incoming Current	2	1
Albedo	1	C^a

2.4 Thermal-Hydraulic Feedback Model

2.4.1 The WIGL Model

Since the SRS reactors are low pressure, low temperature reactors, moderator outside the fuel, target or control element will be considered to be thermally isolated from the rest of the node. This assumption neglects

---

[a] C is a constant relating the actual incoming current to the flux and is defined by

$$C \equiv \frac{J \cdot n}{\varphi}$$

where n is an inward-directed normal on the reactor surface.

reaction and γ-heating in the moderator and hence any moderator feedback effect. However, it simplifies the problem and makes the thermal-hydraulic node different from the neutronic one. Two typical thermal-hydraulic nodes for tritium and plutonium production are shown in Figure (2.5). From the figure we can see that they basically consist of a number of concentric cylinders that contain fuel(target) material and separated by heavy water coolant channels. We use the WIGL thermal-hydraulic model to analyze the thermal part of the problem.

The WIGL thermal-hydraulic feedback model is a simple, constant pressure, one-dimensional (parallel channel) thermal-hydraulic model. It has three primary quantities of interest in each node: the average fuel temperature, the average coolant temperature, and the average coolant density. By performing a static energy balance on the fuel and the coolant in node-l and by assuming that no boiling occurs, the following equations can be derived:

$$\overline{T}_f^l = \overline{T}_c^l + (1 - r)\, q^l \frac{}{V_c^l}\left[\frac{1}{A_h U} + \frac{1}{A_h h_0}\right] \qquad (2.30)$$

$$\left(\overline{T}_f^l - \overline{T}_c^l\right)\left[\frac{1}{A_h U} + \frac{1}{A_h h_0}\right]^{-1} + r\, q^l \frac{V_f^l}{V_c^l} + \frac{2W_c^l C_c}{V_c^l}\left(\overline{T}_i^l - \overline{T}_c^l\right) = 0 \qquad (2.31)$$

and

$$\overline{T}_i^l = 2\overline{T}_c^m - \overline{T}_i^m \qquad (2.32)$$

where

$\overline{T}_f^l$ ≡ average fuel temperature in node-l

$\overline{T}_c^l$ ≡ average coolant temperature in node-l

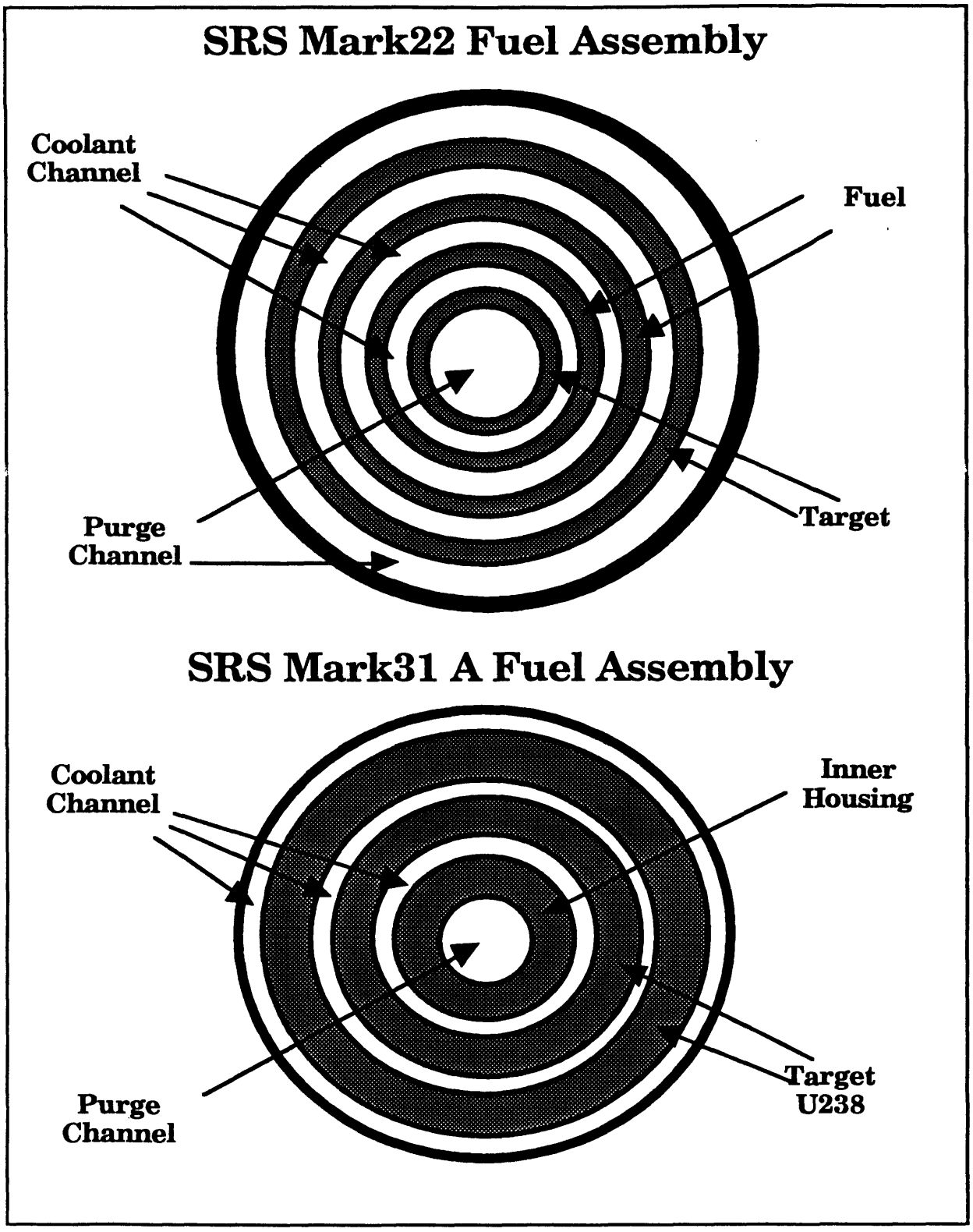

Figure (2.5) Two typical thermal-hydraulic nodes for plutonium and tritium production.

$\overline{T}_i^l$ ≡ inlet coolant temperature of node-*l*

r ≡ fraction of fission power which is deposited directly into coolant

q^l ≡ volumetric energy generation rate in node-*l*

V_c^l ≡ volume of coolant in node-*l*

V_f^l ≡ volume of fuel in node-*l*

A_h ≡ total heat transfer area/total coolant volume within a node

h_0 ≡ heat transfer coefficient

U ≡ conductivity/conduction lengths of the fuel, gap, and cladding(i.e., the inverse of the resistance of heat flow),

C_c ≡ specific heat of the coolant,

W_c^l ≡ coolant mass flow rate through node-*l*.

The above three equations are solved directly for the two unknowns; the average coolant temperature, the average fuel temperature for all nodes in the reactor. Then, the average coolant density is evaluated for all nodes using FLOWTRAN subroutine that utilizes explicit correlations based on the average coolant temperatures with uniform pressure assumed throughout the reactor core.

2.4.2 Cross Section Feedback

Feedback from the thermal-hydraulic equations to the neutronic equations is accomplished by assuming that all macroscopic cross sections (and inverse diffusion coefficients) are linear functions of the three-hydraulic variables. That is, the cross sections are assumed to obey equations of the form

$$\bar{\Sigma}_\alpha^l = \bar{\Sigma}_\alpha^{l^*} + \frac{\partial \bar{\Sigma}_\alpha}{\partial \bar{T}_c}\left(\bar{T}_c^l - \bar{T}_c^*\right) + \frac{\partial \bar{\Sigma}_\alpha}{\partial \bar{T}_f}\left(\bar{T}_f^l - \bar{T}_f^*\right) + \frac{\partial \bar{\Sigma}_\alpha}{\partial \bar{\rho}_c}\left(\bar{\rho}_c^l - \bar{\rho}_c^*\right) \qquad (2.33)$$

where the starred quantities refer to references conditions.

It should be recognized that the partial derivatives w.r.t. average coolant and fuel temperatures and average coolant density are changes in cross section for the entire node including the isolated moderator. In the next chapter a description of a numerical procedure to incorporate the feedback option in the solution will be given.

2.5 Summary

The goal of this chapter was to derive the static, three-dimensional (hex-z), few-group nodal diffusion equations with thermal-hydraulic feedback option. An arbitrary number of energy groups and upscattering in thermal groups were allowed for. For the sake of simplicity, a two-dimensional model was discussed first, then it was extended to obtain three-dimensional results to be incorporated in a computer code the outlines of which will be given in the next chapter. A simple, constant pressure, one-dimensional (parallel channel) thermal-hydraulic model was described. A separate two-dimensional, few-group, finite-difference nodal diffusion model for triangular-shaped nodes will be outlined in the next chapter. The triangular-shaped nodes are required for the calculation of discontinuity factors and for obtaining a fine-mesh, finite difference solution to serve as a reference.

CHAPTER THREE

NUMERICAL SOLUTION METHOD FOR THE STATIC NEUTRON DIFFUSION EQUATION AND APPLICATIONS

3.1 Introduction

In Chapter(2), the static, three-dimensional (hex-z), few-group nodal diffusion equations with a thermal hydraulic feedback option were derived. Also, a separate two-dimensional, few-group, finite-difference nodal diffusion model for triangular-shaped nodes (needed for the calculation of discontinuity factors and for obtaining a fine-mesh, finite-difference solution to serve as a reference) was discussed. The remaining tasks are: 1) develop a numerical solution method by which these equations can be solved, and 2) apply the proposed nodal method to benchmark problems for evaluation and verification purposes.

To understand the nature of the numerical problem, governing equations for both triangular- and hexagonal-shaped-node models should be converted to a matrix form. This will permit a better understanding of the properties of the matrix equations we are dealing with and will finally result in an iteration procedure to be incorporated in a computer code specifically written for those equations. Next, the theory will be applied to two- (hex) and

three-dimensional (hex-z) cores using a two-group analysis which includes upscattering from the thermal group with thermal-hydraulic feedback option. The accuracy of the model is determined by comparison to reference solutions which use the triangular-mesh, finite-difference method.

3.2 Numerical Properties

3.2.1 Triangular-Shaped-Node Model

Part of Section (3.2.1) is taken verbatim from (Gehin, 1990).

Equation (2.10) can be put in the following matrix form

$$[A][\phi] = \frac{1}{\lambda}[M][\phi] \qquad (3.1)$$

where [A] and [M] are square and of order N*G (N is the number nodes) and [ϕ] is a column vector of dimension N*G. As can be seen, Equation (3.1) is in the form of an eigenvalue problem the numerical behavior of which depends on the nature of matrix [A].

In the limit of infinitely-fine mesh spacing, not only is Equation (3.1) guaranteed to converge to the exact solution (Wachspress, 1966) of the diffusion equation, but also the [A] matrix has the following properties:

1. [A] is real and symmetric,
2. the diagonal elements of [A] are positive,
3. the off-diagonal elements of [A] are non-positive,

4. [A] is diagonally dominant, and

5. [A] is irreducible.

A matrix which has these properties is called an S-matrix, and its inverse, $[A]^{-1}$, exists and has all positive elements (Varga, 1962). therefore we may write Equation (3.1) as

$$[\phi] = \frac{1}{\lambda}[R][\phi] \qquad (3.2)$$

where

$$[R] \equiv [A]^{-1}\,[M].$$

Since [M] is a non-symmetric matrix with elements that are either positive or zero, [R] is a non-symmetric non-negative matrix.

With all that in mind, a numerical solution method will be developed in the next section.

Numerical Solution Scheme

The method that will be used to solve Equation (3.2) is standard and comprises of two iterative schemes: outer iterations and inner iterations. In this method no acceleration technique will be used and hence will eliminate most of the complications from the solution method.

Outer Iterations

The solution of Equation (3.2) that we seek is the one with the largest eigenvalue. The solution can be found by using the Power Method (Nakamura, 1986), which can be written as

$$[\phi]^{(t+1)} = \frac{1}{\lambda^{(t+1)}}[R][\phi]^{(t)} \qquad (3.3)$$

and

$$\lambda^{(t+1)} = \lambda^{(t)} \frac{\langle [W], [\phi]^{(t+1)} \rangle}{\langle [W], [\phi]^{(t)} \rangle}; \; t = 1, 2, ..., \infty \qquad (3.4)$$

where t is the iteration number and [W] is a weighting vector. The selection of the weighting vector is arbitrary, but does affect the convergence rate of $\lambda^{(t+1)}$. One common choice is to set the elements of [W] to unity so that the inner products in Equation (3.4) perform a simple summation of the elements of $[\phi]^{(t+1)}$ and $[\phi]^{(t)}$. Using $[\phi]^{(t)}$. as weight function, however, improves the convergence rate by a factor of two over that of a sum vector (Nakamura, 1986).

The iteration is terminated when the following convergence criteria are satisfied

$$|\lambda^{(t+1)} - \lambda^{(t)}| < \varepsilon_\lambda$$

and

$$\max_i \frac{|\phi_i^{(t+1)} - \phi_i^{(t)}|}{\phi_i^{(t)}} < \varepsilon_\phi$$

where $\phi_i^{(t)}$ is the i^{th} element of the vector $[\phi]^{(t)}$ and ε_λ and ε_ϕ are small, pre-selected values.

According to the Perron-Frobenius Theorem (Varga, 1962), an irreducible matrix having non-negative elements has a single positive

eigenvalue greater in value than the modulus of any eigenvalue of the matrix. It is this positive eigenvalue and the corresponding positive eigenvector that we are interested in. Using this theorem and the properties of [R] matrix given in the previous section it is possible to show that the power method outlined in Equations (3.3) and (3.4) are guaranteed to converge to the largest positive eigenvalue and the unique positive eigenvector (Nakamura, 1986).

Inner Iterations

Since the [A] matrix may be large, its inversion required to determine [R] may not be practical. Therefore at each outer iteration, the new flux vector [ϕ] in Equation (3.3) must be determined iteratively. The method used to perform this inner iteration will be the Gauss-Seidel Method (Varga, 1962).

We begin the application of this method by defining an additional vector known as the fission source vector

$$[F] \equiv \frac{1}{\lambda}[M][\phi] \qquad (3.5)$$

Using this definition, the original equation can be written as

$$[A]\,[\phi] = [F] \qquad (3.6)$$

In the Gauss-Seidel Method the coefficients matrix, [A], is broken into three separate matrices

$$[A] = [A_d] + [A_l] + [A_u] \qquad (3.7)$$

where $[A_d]$ is a diagonal matrix, $[A_l]$ is a strictly lower matrix and $[A_u]$ is a strictly upper matrix. Using q as an iteration index we can write the inner iteration procedure for outer iteration (t + 1) as

$$[\phi]^{(t+1,\,q+1)} = ([A_d] - [A_l])^{-1}[A_u][\phi]^{(t+1,\,q)} + ([A_d] - [A_l])^{-1}[F]^{(t+1)}. \qquad (3.8)$$

The fission source vector for outer iteration (t + 1) is given by

$$[F]^{(t+1)} = \frac{1}{\lambda^{(t+1)}}[M][\phi]^{(t)} \qquad (3.9)$$

The initial flux vector, $[\phi]^{(t+1,\,0)}$, used in the procedure is the eigenvector from the previous outer iteration, $[\phi]^{(t)}$. Generally, it is necessary to fully converge the flux vector in the inner iteration. In most situations, more than three iterations provides little improvement in the rate of convergence of the overall iterative procedure (Gehin, 1990).

Summary of the Iterative Method

A flow diagram of the iterative method is given in Figure (3.1). The general scheme proceeds as follows

1. An initial guess is made for the flux vector $[\phi]^{(t)}$. (Usually all elements are set equal to 1.)

2. From this guess the eigenvalue, $\lambda^{(t+1)}$, and the fission source,

$[F]^{(t+1)}$, are calculated.

3. Several inner iterations are performed to calculate a new flux vector $[\phi]^{(t+1)}$.

4. With the new flux vector, we repeat the process starting with step 2 until the eigenvalue and the flux vector converge.

3.2.2 Hexagonal-Shaped-Node Model

The equivalent of Equation (3.1) for the hexagonal geometry is deduced from Equation (2.24) and can be written as

$$[A'][\phi] = \frac{1}{\lambda}[M'][\phi] + [C][J] \qquad (3.10)$$

and

$$[J] = [C][J] + [A''][\phi] + \frac{1}{\lambda}[M''][\phi] \qquad (3.11)$$

where [A'], [A''], [M'], [M''], and [C] are square matrices and of order N*G and $[\phi]$ and [J] are column vectors of dimension N*G. Equations (3.10) and (3.11) form a system that cannot be directly solved using the simple technique explained in the previous section. In other words, if we used equation (3.10) to solve for $[\phi]$ and λ by inverting [A'], we would still need to determine [J] to evaluate the second part of the right hand side of Equation (3.10). To get [J], from Equation (3.11), we need to determine $[\phi]$ and the system eigenvalue, λ. However, if the problem is broken into two parts, namely Equation (3.10) and Equation (3.11), an iteration procedure can be devised to enable the solution of the nodal balance equation in the hexagonal geometry.

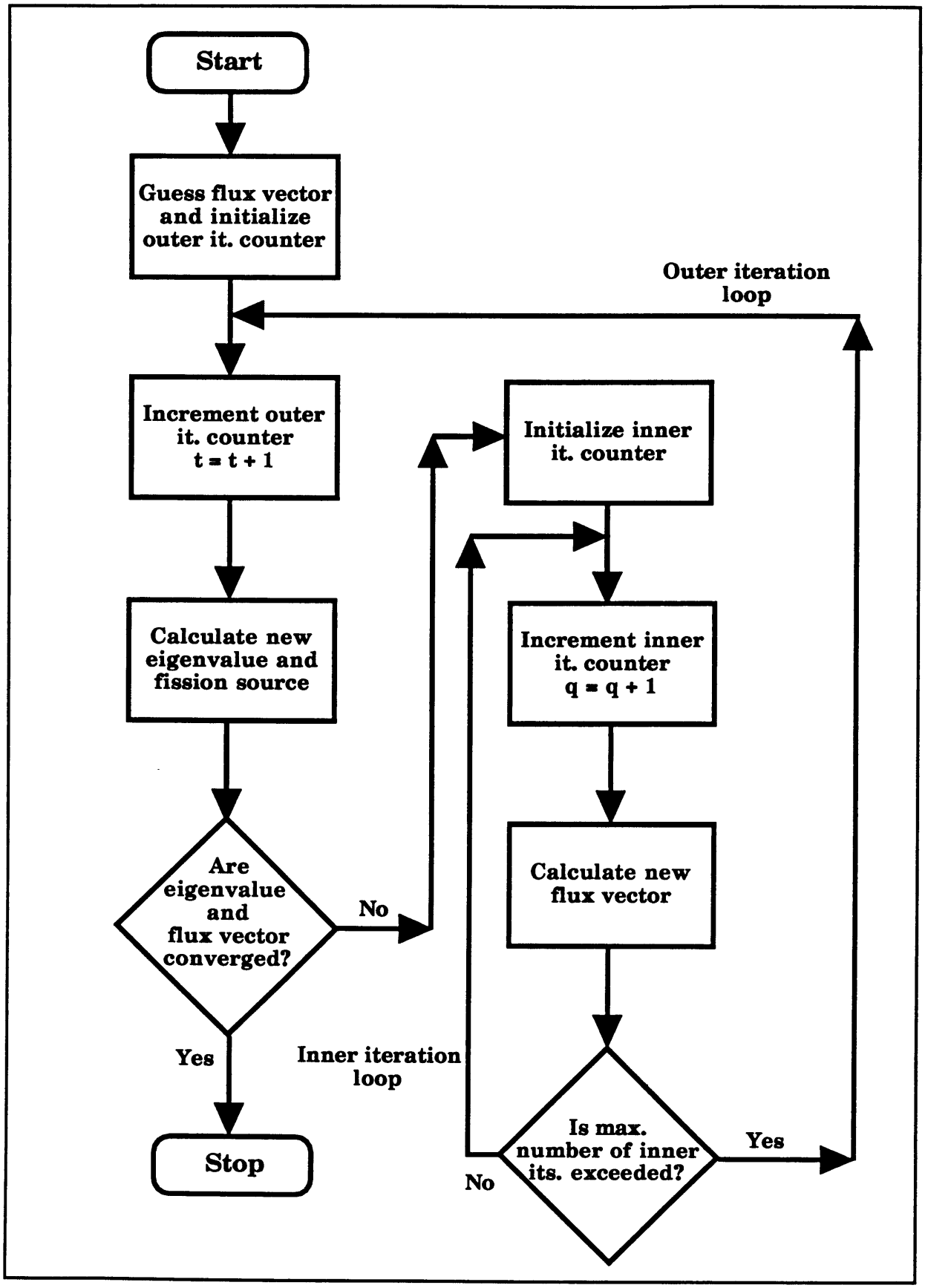

Figure (3.1) Flow diagram of iterative solution method (from Gehin, 1990).

Numerical Solution Scheme

The method that will be used to solve Equations (3.10) and (3.11) comprises three iterative schemes: fission source iterations, flux iterations, and current iterations. In this method acceleration techniques will be used for fission source iterations and for flux iterations while current iterations will remain unaccelerated for reasons will be obvious in the coming sections.

Fission Source Iterations

The solution to Equation (3.1) can be found by using the Power Method (Nakamura, 1986), which can be written as

$$[\phi]^{(t+1)} = \frac{1}{\lambda^{(t+1)}}[A']^{-1}[M'][\phi]^{(t)} + [A']^{-1}[C][J] \qquad (3.12)$$

and

$$\lambda^{(t+1)} = \lambda^{(t)} \frac{\langle [W], [\phi]^{(t+1)} \rangle}{\langle [W], [\phi]^{(t)} \rangle}; \; t = 1, 2, ..., \infty \qquad (3.13)$$

where t is the iteration number and [W] is a weighting vector. The selection of the weighting vector is arbitrary, but does affect the convergence rate of $\lambda^{(t+1)}$. One common choice is to set the elements of [W] to unity so that the inner products in Equation (3.4) perform a simple summation of the elements of $[\phi]^{(t+1)}$ and $[\phi]^{(t)}$. Another choice is to use [I][M'] as a weight function where [I] is the identity row vector (Hageman, 1981). This turned out to accelerate the above iterative scheme the most.

The successive calculations of the fission source vary in the asymptotic limit by an amount governed by the dominance ratio

$$d = \left| \frac{\lambda}{\lambda_1} \right|,$$

where λ and λ_1 are the fundamental and first harmonic eigenvalues, respectively, of the iteration matrix of Equation (3.12). This ratio, which in general varies from iteration to iteration, will be close to unity for most problems, resulting in slow convergence.

Wielandt's method of fractional iteration (Wachspress, 1966), or eigenvalue shifting, is one method for accelerating the convergence of the outer iterations. It does that by effectively reducing the dominance ratio, and this can be seen by changing Equation (3.10) to

$$\left[[A'] - \frac{1}{\lambda_s} [M'] \right] [\phi] = \left(\frac{1}{\lambda} - \frac{1}{\lambda_s} \right) [M'][\phi] + [C][J] \qquad (3.14)$$

where λ_s is arbitrarily selected but subject to certain restrictions discussed below.

According to the new scheme Equations (3.12) and (3.13) will become

$$[\phi]^{(t+1)} = \left(\frac{1}{\lambda^{(t+1)}} - \frac{1}{\lambda_s^{(t)}} \right) \left[[A'] - \frac{1}{\lambda_s^{(t)}} [M'] \right]^{-1} [M'][\phi]^{(t)} + \left[[A'] - \frac{1}{\lambda_s^{(t)}} [M'] \right]^{-1} [C][J] \qquad (3.15)$$

$$\left(\frac{1}{\lambda^{(t+1)}}-\frac{1}{\lambda_s^{(t)}}\right)^{-1}=\left(\frac{1}{\lambda^{(t)}}-\frac{1}{\lambda_s^{(t-1)}}\right)^{-1}\frac{\left\langle [W],[\phi]^{(t+1)}\right\rangle}{\left\langle [W],[\phi]^{(t)}\right\rangle};\ t=1,2,\ldots,\infty \qquad (3.16)$$

and

$$\frac{1}{\lambda^{(t+1)}}=\frac{1}{\lambda_s^{(t)}}+\left(\frac{1}{\lambda^{(t+1)}}-\frac{1}{\lambda_s^{(t)}}\right) \qquad (3.17)$$

Note that if $1/\lambda_s$ is closer to $1/\lambda$, than $1/\lambda_1$, the converged eigenvalue and eigenvector will be identical to that obtained using the Power Method. In general, λ_s is required to be greater than the largest λ. In practice λ_s is assumed to be constant throughout the iteration procedure so that additional complications of updating the shifted eigenvalue could be avoided. The shifted dominance ratio is given by

$$d_s=\frac{\left|\frac{1}{\lambda}-\frac{1}{\lambda_s}\right|}{\left|\frac{1}{\lambda_1}-\frac{1}{\lambda_s}\right|},$$

which is clearly smaller than the unshifted dominance ratio if λ_s is greater than or equal to λ. Therefore, the convergence of the outer iterations will be accelerated using Wielandt's method. The Power Method may be obtained from Wielandt's Method by setting λ_s equal to infinity.

The fission source vector defined as

$$[F']\equiv\frac{1}{\lambda}[M][\phi] \qquad (3.18)$$

can now be updated according to

$$[F']^{(t+1)} = \frac{1}{\lambda^{(t+1)}}[M'][\phi]^{(t)} \qquad (3.19)$$

The iteration is terminated when the following convergence criteria are satisfied

$$|\lambda^{(t+1)} - \lambda^{(t)}| < \varepsilon_\lambda$$

and

$$\max_i \frac{|\phi_i^{(t+1)} - \phi_i^{(t)}|}{\phi_i^{(t)}} < \varepsilon_\phi$$

where $\phi_i^{(t)}$ is the i^{th} element of the vector $[\phi]^{(t)}$ and ε_λ and ε_ϕ are small, pre-selected values.

Flux Iterations

As in the triangular-shaped-node model, we shall use the Gauss-Seidel method which will be accelerated using the Successive Over Relaxation technique.

Equation (3.10) can be rewritten as

$$[A'][\phi] = [F'] + [C][J] \qquad (3.20)$$

which is solved using the method discussed earlier to yield

$$[\phi]^{(t+1,\,q+1)} = ([A_d'] - [A_l'])^{-1}[A_u'][\phi]^{(t+1,\,q)} + ([A_d'] - [A_l'])^{-1}[F]^{(t+1)} + ([A_d'] - [A_l'])^{-1}[C][J] \tag{3.21}$$

The initial flux vector, $[\phi]^{(t+1,\,0)}$, used in the procedure is the eigenvector from the previous outer iteration, $[\phi]^{(t)}$. Generally, it is not necessary to fully converge the flux vector in the flux iteration. In most situations, more than one iteration provides little improvement in the rate of convergence of the overall iterative procedure.

The convergence of the flux iterations is accelerated by applying the Successive Over Relaxation (SOR) technique to the Gauss-Seidel Method. The basic idea is that a combination of the value of the flux vector at the current iteration and its value in the previous iteration is all that is needed to accelerate the convergence of the flux iterations. This can be expressed as

$$[\phi^*]^{(t+1,\,q+1)} = (1 - r)\,[\phi^*]^{(t+1,\,q)} + r\,[\phi]^{(t+1,\,q+1)}$$

where r is a relaxation parameter that has a value between 1 an 2 and has to be pre-selected before the iteration procedure begins. Strictly speaking, r should be different for each energy group and, in principle, can be calculated from the observed behavior of the iteration process. However, experience with heavy water reactor problems suggests that r can be taken as a constant in the range of 1.3 -1.5.

Current Iterations

Up to this point the current column vector, [J], has been taken to be constant throughout the inner and the outer iterations. The situation thus

resembles a fixed source problem for which we have a source of neutrons that contributes independently to the balance of the neutron population in the system. However, although we chose the current vector to be constant throughout the iteration process, it is in fact a dependent contributor to the overall balance of Equations (3.10) and (3.11). Equation (3.11) suggests a straight forward method by which we can evaluate the current column vector once we have calculated the flux column vector from the flux iterations.

The proposed iteration procedure will look like

$$[J]^{(m+1)} = [C][J]^{(m)} + [A'']\left[\phi\right]^{(t+1,\,q+1)} + \frac{1}{\lambda^{(t+1)}}[M'']\left[\phi\right]^{(t+1,\,q+1)} \qquad (3.22)$$

where m is the iteration number. This iteration procedure does not need any acceleration; one current iteration per fission source iteration is quite sufficient.

Summary of the Iterative Method

A flow diagram of the iterative method is given in Figure (3.2). The general scheme proceeds as follows

1. An initial guess is made for the flux vector $[\phi]^{(t)}$. (Usually all elements are set equal to 1.)
2. From this guess the eigenvalue, $\lambda^{(t+1)}$, and the fission source, $[F]^{(t+1)}$, are calculated.
3. Several flux iterations (usually one per fission source iteration) are performed to calculate a new flux vector $[\phi]^{(t+1)}$.

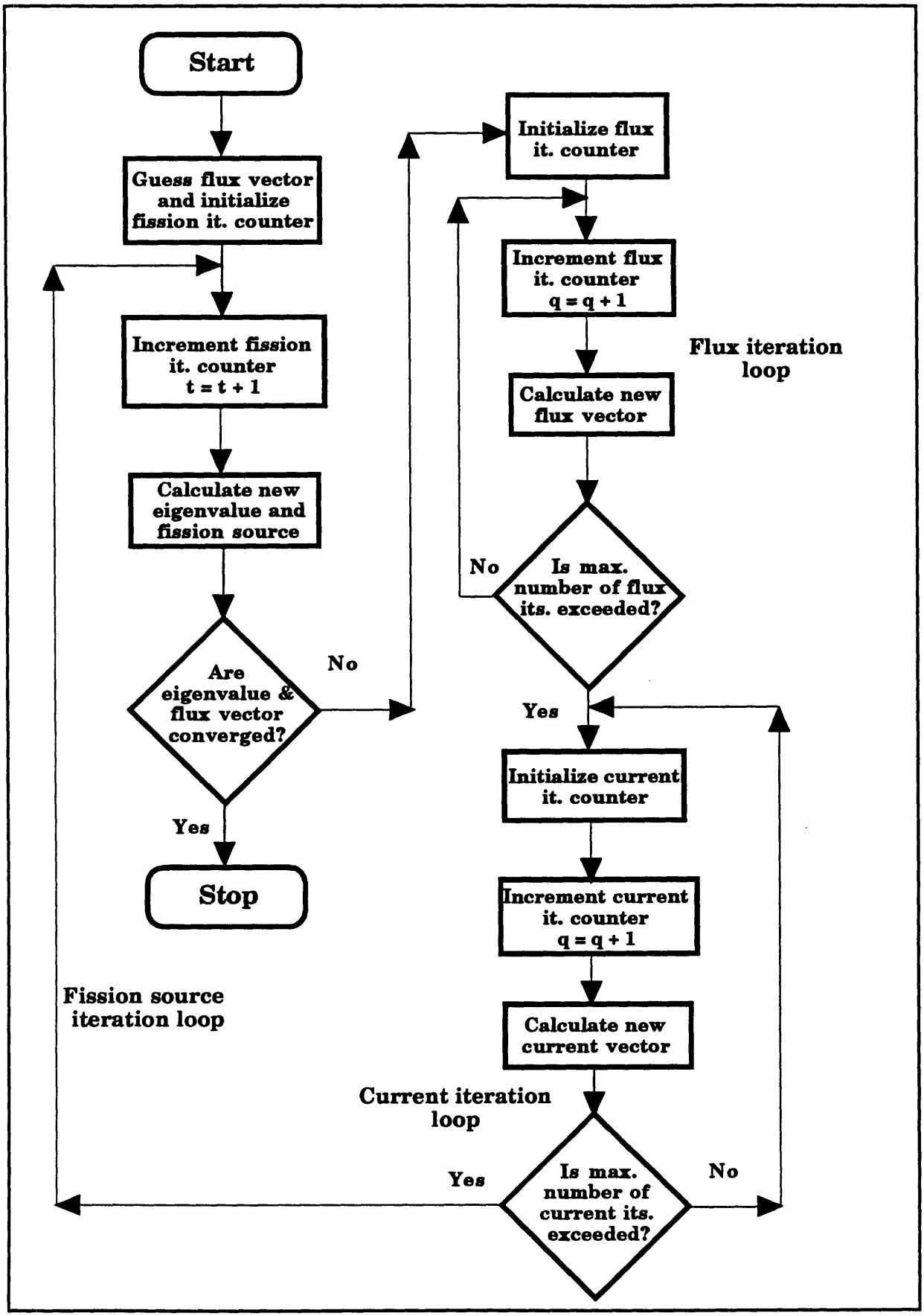

Figure (3.2) Flow diagram of iterative solution method.

4. Several current iterations (usually one per fission source iteration) are performed to calculate a new current vector $[J]^{(t+1)}$.
5. With the new flux and current vectors, we repeat the process starting with step 2 until the eigenvalue and the flux vector converge.
6. If thermal-hydraulic feedback option is chosen, the new flux and current vectors are used to update the cross sections according the core power level. Then the process is repeated starting with step 2 until the eigenvalue and the flux vector converge.

3.3 Applications

The accuracy of the nodal model described in the preceding sections has been tested numerically by comparison with a number of reference calculations. A computer code (referred to as '**MITHEX-Z**') has been written in standard FORTRAN 77 to carry out these tests and perform numerical analysis of the proposed nodal model. MITHEX-Z is a workstation-based computer code that allows an arbitrary number of energy groups and upscattering. It solves eigenvalue as well as transient problems with a thermal-hydraulic feedback option. The results of these numerical tests will be presented for two kinds of applications: 1) applications involve problems without thermal-hydraulic feedback, and 2) applications involve problems with thermal-hydraulic feedback.

3.3.1 Applications without Thermal-Hydraulic Feedback

The largest of these tests, designated as ANL-Mark22 problem,

involves a three-dimensional (hex-z), two-group simulation of a heavy water reactor of the Savannah River type. Figure (3.3) gives an over view of one-sixth of a cross sectional area of the reactor. From the figure, we can see that the core is composed of homogenized hexagons (about 18 cm across flats) and has 60^0-degree rotational symmetry. Also, the core is heterogeneous in the z-direction but is symmetric around the mid-plane. It has zero-flux boundary condition in both axial and transverse directions. Material specifications and core dimensions are given in Appendix A. Tests results are appear in Table (3.1).

The DIF3D and reference calculations were performed at the Argonne National Laboratory. The DIF3D quadratic model is somewhat more complicated computationally than the MIT quadratic model. However, both quadratic models have 27 times fewer unknown fluxes to find than the 6-triangle/hex finite-difference scheme and hence for the same accuracy, should be considerably faster (Shatilla and Henry, 1992).

Table (3.1) Accuracy of various models as applied to the simulation of a heavy water production reactor (From Shatilla and Henry, 1992).

	Quadratic Models*		Finite-Difference Model**	
	MIT 8Z/4Z	DIF3D	6T's/hex	24T's/hex
Error in K_{eff} %	-0.39/-0.42	-0.203	-0.211	-0.062
Max. Error in Assembly Power %	-1.38/-1.39	1.03	1.98	0.51
Avg. Error in Assembly Power %	0.59/0.55	----	----	----
Execution Time (sec)	3600/1800***	3.9#	----	----

* 1 unknown/hexagon; 8 axial segments (MIT model, 16 (or 8) axial segments)
** DIF3D; 36 axial segments
*** On IBM RISC/6000; convergence = 10^{-7} for K_{eff}, 10^{-5} for flux.
# On ANL Cray X-MP; convergence = 10^{-7} for K_{eff}, 10^{-5} for flux.

Cross Section Set by Planar Region

and Axial Segment

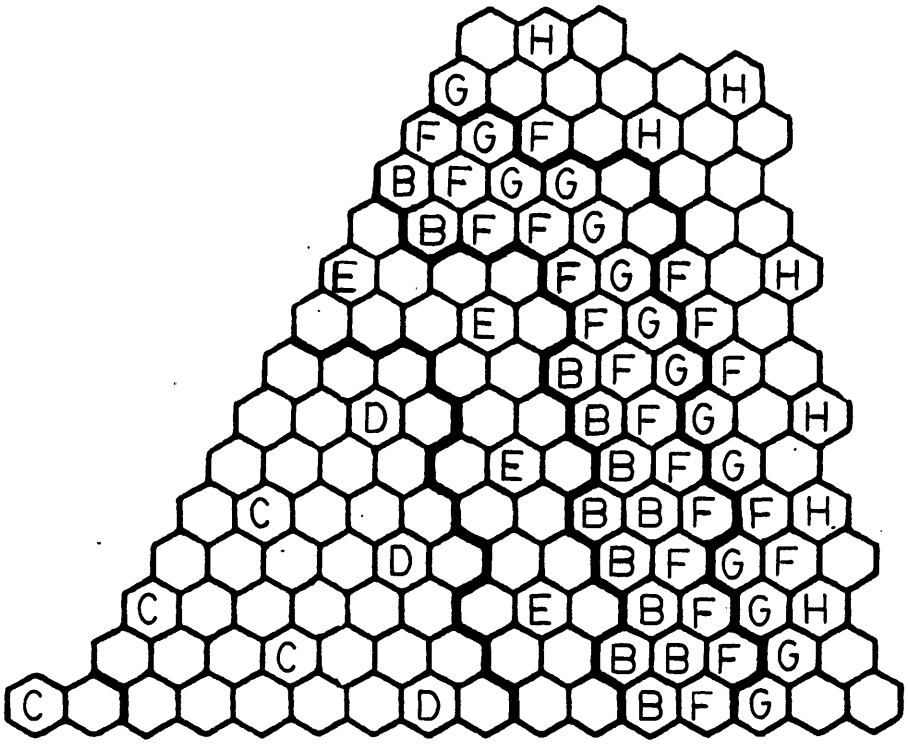

	Axial Segment	
	Segment 1 [0, H/4]	Segment 2 [H/4, H/2]
Planar Region		
A (Flat Zone Core)	2	2
B (Buckled Zone Core)	6	6
C (Gang 1 - Control)	1	11
D (Gang 2 - Control)	4	12
E (Gang 3 - Control)	5	13
F (D_2O - Vacancies)	7	7
G (Blanket)	8	8
H (Thermal Shield)	9	9

Figure (3.3) ANL-Mark22 reactor geometry and material specifications.

We conclude from Table (3.1) that the MIT simplified quadratic model is reasonably accurate. The MIT model may be slower than the DIF3D model. However, it is difficult to come up with a definitive conclusion based on the above table since the two machines used in the comparison are totally different, and the MIT calculations were done for the whole core whereas the ANL calculations were done for one-sixth of the core.

To test further the accuracy of the quadratic model and to examine improvements brought about by the use of discontinuity factors, a much smaller two-dimensional benchmark problem was analyzed. The geometry is shown in Figure (3.4). As can be seen, the core, (D_2O moderated and reflected) is made of "supercells" (or "patches"), each patch consisting of a control hexagon (about 18 cm across flats) surrounded symmetrically by three target hexes and three fuel hexes. The core was subject to zero-incoming current boundary condition (Shatilla and Henry, 1992).

Cores made up of both homogeneous and heterogeneous hexes were analyzed. For the homogeneous cases each control, fuel and target hexagon was partitioned with 24 equilateral triangles, the central six being homogeneous control, fuel or target material and the remaining 18 being D_2O (See Figure (3.4). Material specifications and properties are given in Appendix A.

Two-group infinite lattice calculations with 24 triangles per hexagon were run to obtain homogenized cross sections and discontinuity factors for the individual, heterogeneous control, target, and fuel hexes. These values were then used for the full core, nodal calculations. Full core reference

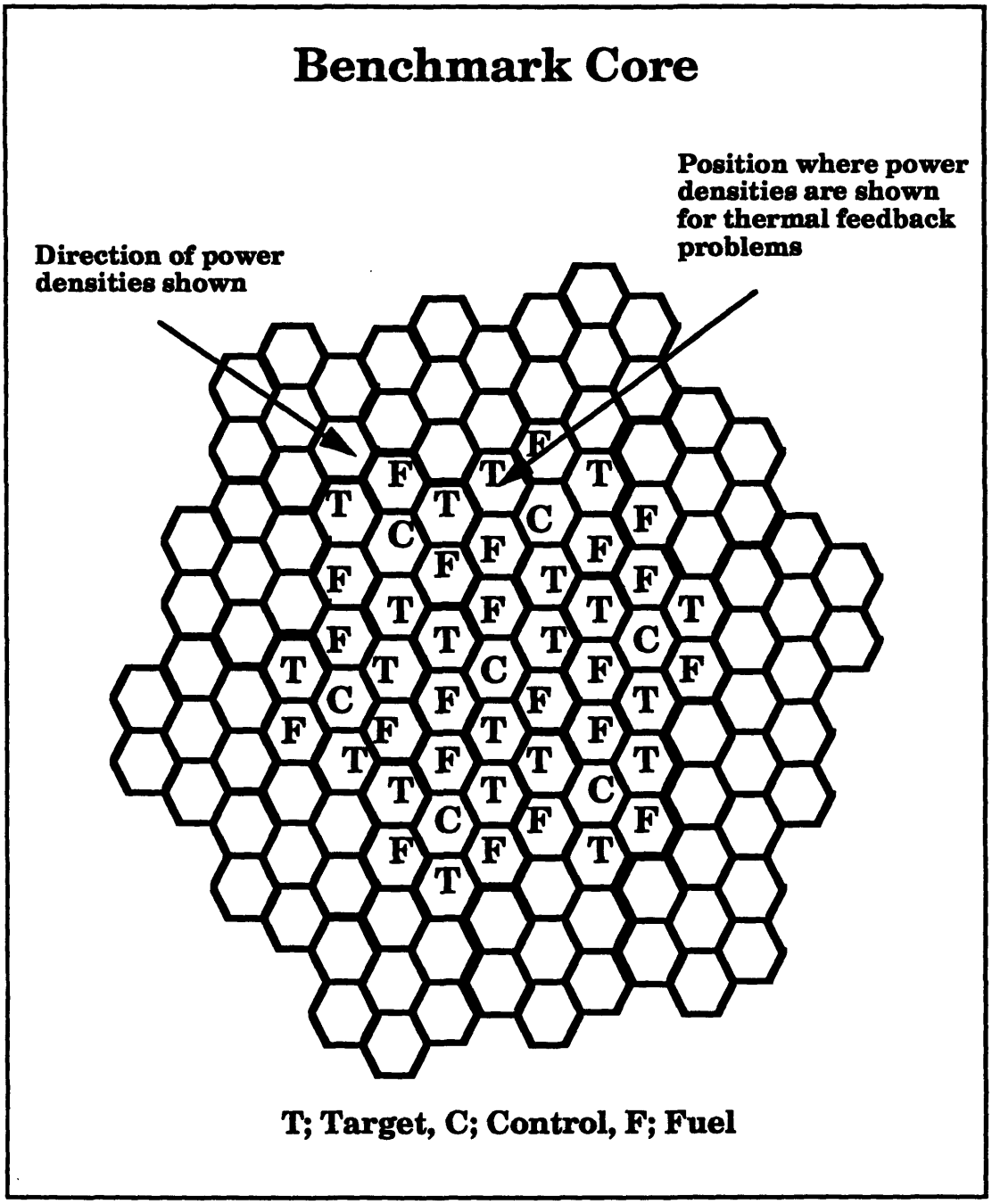

Figure (3.4) Cross sectional area of the core used for the benchmark problem.

results for all cases were obtained 24 triangles per hex using MITHEX (Gehin, 1990).

Table (3.2) shows results for cores composed of both homogeneous and heterogeneous nodes. Both finite-difference and quadratic nodal calculations were run with one mesh box per hexagon.

Table (3.2) Comparisons of quadratic and finite-difference results (From Shatilla and Henry, 1992).

	Finite-Difference Model			Quadratic Model		
	Hom;1	**Het;1**	**Het;i**	**Hom;1**	**Het;1**	**Het;i**
Error in K_{eff} %	1.86	2.54	0.10	-0.66	-0.005	-0.4
Max. Error, Nodal Power %	-13.7	-10.6	-5.02	2.39	3.74	1.80
Avg. Error, Nodal Power %	7.28	5.95	1.81	0.96	1.73	0.90
Execution Time, (s)	2.5	2.5	2.5	25	25	25[a]

Hom ≡ Homogeneous nodes; Het ≡ Heterogeneous nodes; 1 ≡ Unity discontinuity factors used; i ≡ Infinite-lattice discontinuity factors used.
a : Using IBM RSIC/6000.

We conclude from the cases run for homogeneous nodes that the simple quadratic nodal method provides a substantial improvement over the finite-difference method with one mesh box per hexagon. Whether homogenized cross sections and discontinuity factors found from infinite lattice calculations provide acceptable accuracy for the quadratic model remains an open question. The small benchmark problems provides a very severe test, since the reflector region influences the entire core. However, the heterogeneities are mild, and, since the infinite lattice calculations were run only with two-group diffusion theory, they provide no test of transport or multigroup spectral effects. More work is called for on this question (Shatilla and Henry, 1992).

Also, as can be seen from Table (3.2), the simplified quadratic model is slower than the finite-difference model. This can be attributed to the fact that the number of unknowns per node per energy group is approximately nine times that of the finite-difference model.

To evaluate the thermal-hydraulic feedback model incorporated in the code, a one-dimensional problem was run. The core consists of 9 homogenized nodes (20 cm each). The three middle nodes simulate fuel material whereas the rest are target material. Zero-flux boundary conditions are imposed on the core boundaries. Material specifications are given in Appendix A. First the code was tested with the thermal-hydraulic feedback turned off. Figure (3.5) shows normalized power densities across the length of the reactor compared to results obtained from an independent nodal code, CONQUEST (Gehin, 1992). The excellent agreement for the power densities is evident. The two calculations agreed in eigenvalue to the sixth decimal place. This result provides another test of the code without feedback.

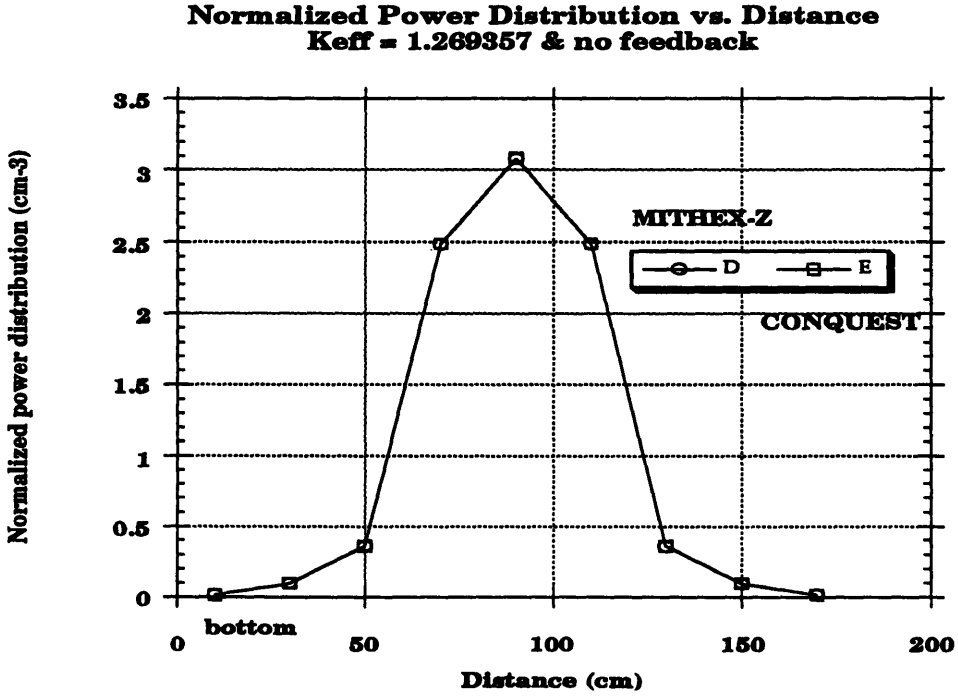

Figure (3.5) One-dimensional problem results.

3.3.2 Applications with thermal-hydraulic feedback

A three-dimensional core with a cross sectional area similar to that shown in Figure (3.4) was used to verify the accuracy of the thermal-hydraulic feedback component of the code. One-third of each of the five radial planes (each 20 cm high) was assumed to contain fuel only. The reason for this choice was to test how effectively thermal-hydraulic feedback will reduce local power. Material specifications and thermal-hydraulic feedback parameters are given in Appendix A. Figure (3.6) shows normalized power densities along the length of the core (100 cm) at the target node position indicated in Figure (3.4). As can be seen from the figure, since the core has a negative power reactivity coefficient, the axial power shape experiences a slight shift towards the bottom of the core.

The execution times for both cases, with and without thermal-hydraulic feedback, were the same and approximately equal to 125 s. This indicates that the thermal-hydraulic feedback calculations, because of their relative simplicity, take comparatively negligible time to be execute.

Figure (3.7) shows power densities transversing seven radial nodes at the last axial plane located at the core exit (see Figure (3.4)). The power density change is only slightly altered by the thermal feedback effects.

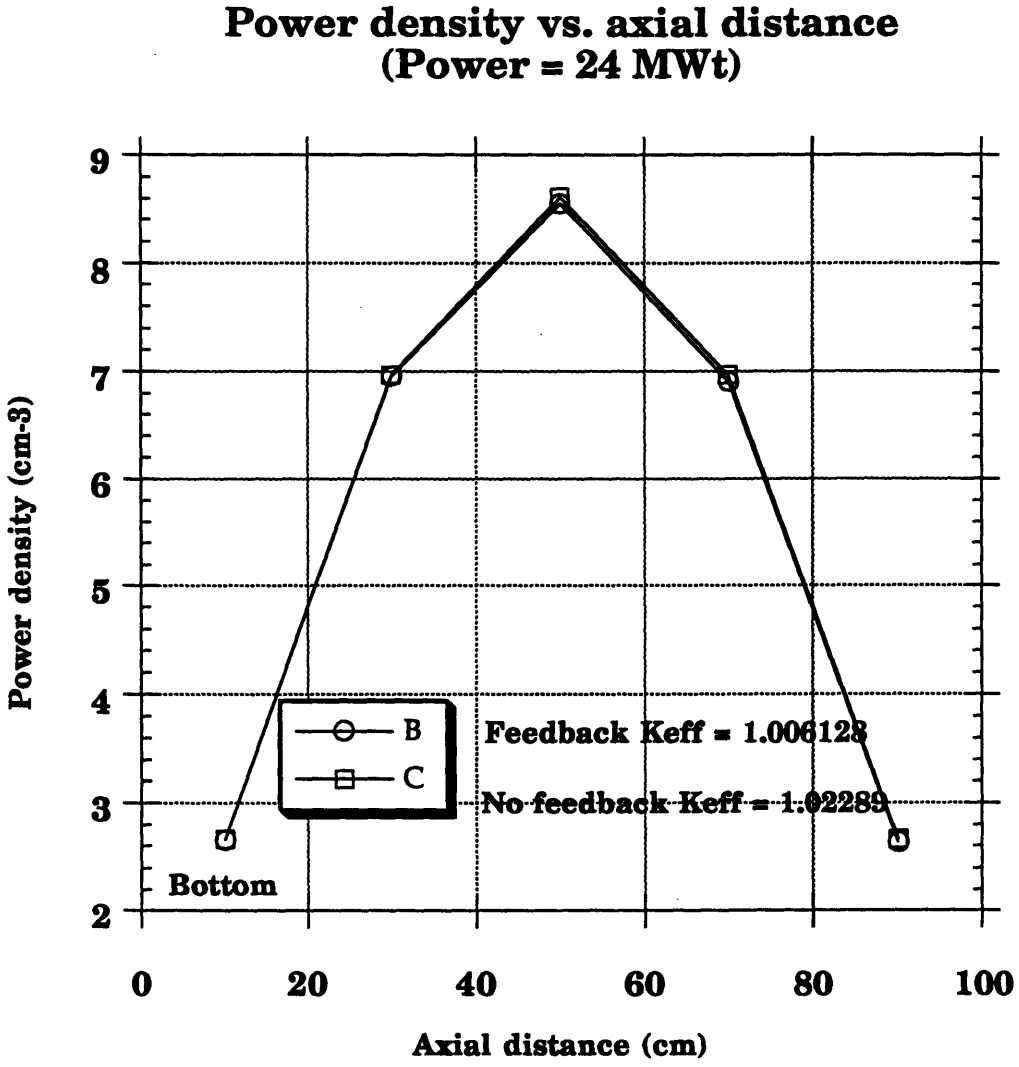

Figure (3.6) Power density vs. axial distance.

Finally the one-dimensional problem described in the previous section was run again but with thermal-hydraulic feedback option turned on. Material specifications and thermal-hydraulic parameters are given in Appendix A. Figure (3.8) shows excellent agreement of normalized power densities with those calculated using CONQUEST (Gehin, 1992). The eigenvalues for the two calculations agree through the sixth decimal place.

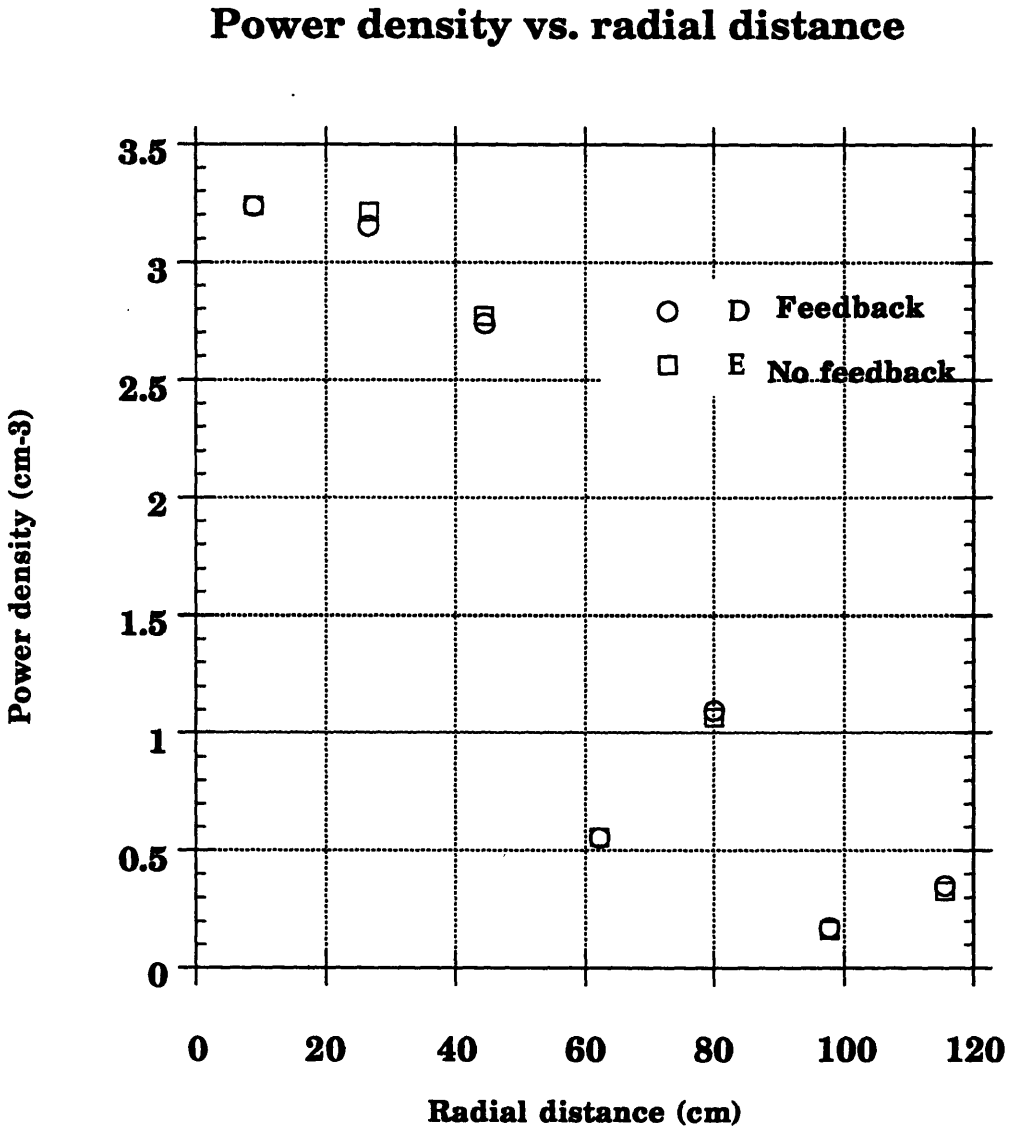

Figure (3.7) Power densities vs. radial distance (power fluctuations).

We conclude from the above tests that the thermal-hydraulic feedback component of the code is working as it should and shows excellent agreement when compared to one-dimensional benchmark results.

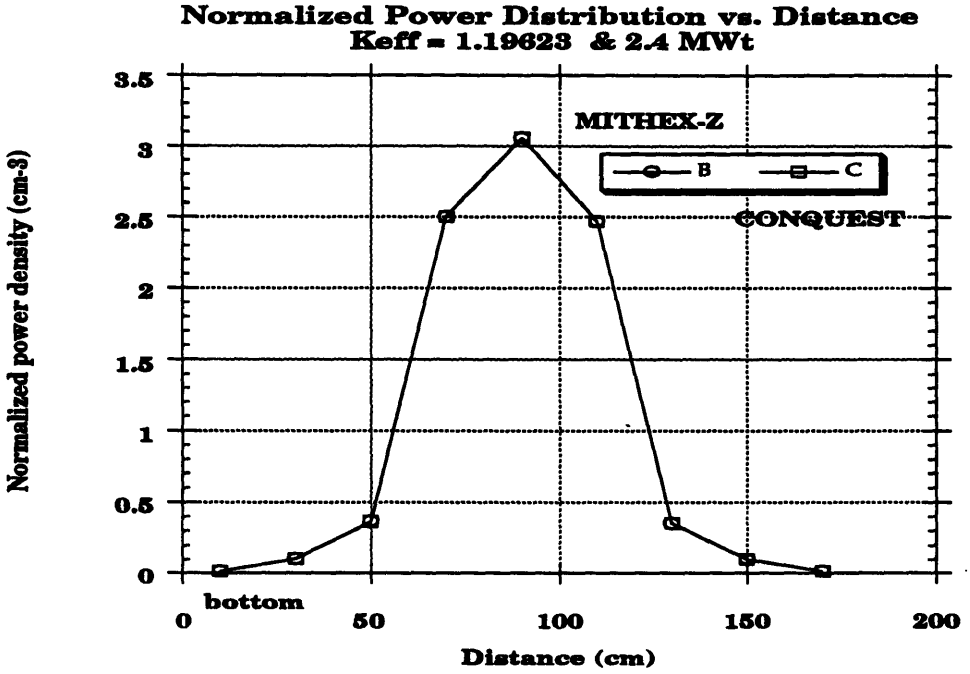

Figure (3.8) One-dimensional problem results (with feedback).

3.4 Summary

In Chapter(2), the static, three-dimensional (hex-z), few-group nodal diffusion equations incorporating a thermal hydraulic feedback option were derived. Also, a separate two-dimensional, few-group, finite-difference nodal diffusion model for triangular-shaped nodes (needed for the calculation of discontinuity factors and for obtaining a fine-mesh, finite-difference solution to serve as a reference) was discussed. In the present chapter a numerical solution method by which these equations can be solved has been developed, and results have been applied to benchmark problems for evaluation and verification purposes. These tests show that the simple quadratic nodal method provides a substantial improvement over the finite-difference method with one mesh box per hexagon. Whether homogenized cross sections and

discontinuity factors found from infinite lattice calculations provide acceptable accuracy for the quadratic model remains an open question. Also, the thermal-hydraulic feedback component of the code is working properly and it has an excellent accuracy when compared to one-dimensional benchmark problems. The simplified quadratic model is slower than the finite-difference (one point/hex) model because of the larger number of unknowns to be solved for per node per energy group. However, it is faster and more accurate than the finite difference with 6 triangles/hex.

CHAPTER FOUR

SOLUTION OF THE DYNAMIC NEUTRON DIFFUSION EQUATION

4.1 Introduction

The goal of this chapter is to derive the time-dependent, three-dimensional (hex-z), few-group nodal diffusion equations with a thermal-hydraulic feedback option. We shall allow for a general number of energy groups and for upscattering in thermal groups. Finally, a simple, constant pressure, one-dimensional (parallel channel) thermal-hydraulic model will be incorporated.

As in Chapter (2), we begin the derivation by integrating the time-dependent Boltzman transport equation and the time-dependent delayed neutron precursor equations over all directions to obtain a set of equations that relate the scalar flux density to the net current density and to the concentrations of delayed neutron precursors. The resultant equations are then integrated over an energy group and over the volume of the node. The resulting equations are called few-group, time-dependent nodal balance equations which are basically relations between the time-dependent volume-averaged flux for a node, the time-dependent face-averaged currents, and the

time-dependent concentrations of delayed neutron precursors in that node. To solve this set of equations coupling relations that relate the volume-averaged flux and the face-averaged currents are needed. Fick's Law is used to obtain the desired relation. However, using Fick's Law in conjunction with a finite difference or any higher order approximation introduces additional unknowns, namely, the face-averaged fluxes. Again, as in Chapter (2), the face-averaged fluxes are assumed to have a quadratic shape across a given node.

Finally, a time-dependent WIGL (Vota, 1969) thermal-hydraulic model is incorporated as a feedback mechanism to update the time-dependent nuclear cross sections. Time-dependent average fuel and coolant temperatures and time-dependent average coolant density are calculated for each node based on the power level of the system. These three variables are used to update the nuclear parameters of the core by linear interpolation.

4.2 Derivation of the Time-Dependent Nodal Equations

By integrating the time-dependent Boltzman neutron equation and the delayed neutron precursors equations over all directions and over an energy group g it is possible to obtain formally

$$\begin{aligned}\frac{1}{v_g}\frac{d}{dt}\phi_g(\underline{r},t) = &- \nabla.\underline{J}_g(\underline{r},t) - \Sigma_g(\underline{r},t)\phi_g(\underline{r},t) \\ &+ \sum_{g'=1}^{G}\sum_{j}\frac{1}{\lambda}\chi_{pg}^{j}(1-\beta^{j})\nu\Sigma_{fg'}^{j}(\underline{r},t)\phi_{g'}(\underline{r},t) \\ &+ \sum_{i=1}^{I+J}\chi_{ig}\lambda_i\int_{v}K_i(\underline{r},\underline{r}',t)\ c_i(\underline{r}',t)\,dV' \\ &+ \sum_{\substack{g'=1 \\ g'\neq g}}^{G}\Sigma_{gg'}(\underline{r},t)\phi_{g'}(\underline{r},t)\ ;\quad g = 1,2,....,G\end{aligned} \tag{4.1}$$

$$\frac{d}{dt} c_i(\underline{r},t) = \frac{1}{\lambda} \sum_{g'=1}^{G} \sum_{j} \beta_i^j \nu\Sigma_{fg'}^j (\underline{r},t)\phi_{g'}(\underline{r},t) - \lambda_i c_i(\underline{r},t); \quad i = 1,2,..., I + J' \qquad (4.2)$$

and

$$\frac{d}{dt} c_i(\underline{r},t) = \sum_{g'=1}^{G} \Sigma_{cg'}^i (\underline{r},t)\phi_{g'}(\underline{r},t) - \lambda_i c_i(\underline{r},t); \quad i = I + J' + 1,..., I + J \qquad (4.3)$$

where

G ≡ total number of energy groups,

I ≡ total number of delayed fission neutron precursor groups,

J ≡ total number of delayed photoneutron precursor group,

$\phi_g(\underline{r},t)$ ≡ time-dependent group g scalar flux density,

$\underline{J}_g(\underline{r},t)$ ≡ time-dependent group g net current density,

$\Sigma_g(\underline{r},t)$ ≡ time-dependent group g total macroscopic cross section minus the time-dependent group g in-group scattering cross section,

v_g ≡ group-g neutron velocity,

λ ≡ system eigenvalue (K_{eff}) at t = 0,

χ_{pg} ≡ prompt neutron fission spectrum for group g,

χ_{ig} ≡ i^{th} delayed neutron spectrum for energy group g,

λ_i ≡ i^{th} delayed neutron decay constant,

$\nu\Sigma^j_{fg}(\underline{r},t)$ ≡ time-dependent number of neutrons emitted per fission multiplied by the time-dependent macroscopic fission cross section for group g for the j^{th} fissionable isotope,

$c_i(\underline{r},t)$ ≡ time-dependent concentration of the i^{th} delayed neutron precursor,

$K_i(\underline{r},\underline{r}',t)dV$ ≡ probability that a γ-ray emitter at $\underline{r}'$ from the i kind of γ-emitter will result in the isotropic emission of a neutron into dV (i = I + 1, I + 2, ..., I + J),

$\Sigma^i_{cg}(\underline{r},t)$ ≡ time-dependent capture cross section for the i^{th} γ-emitter for energy group g,

β^j_i ≡ fraction of neutrons emitted from the j^{th} fissionable isotope that appear in the i^{th} precursor group,

β^j ≡ fraction of all neutrons emitted from the j^{th} fissionable isotope ($\beta^j = \sum_{i=1}^{I} \beta^j_i$),

$\Sigma_{gg'}(\underline{r},t)$ ≡ time-dependent macroscopic scattering cross section from group g′ to group g.

Note that the fourth term on the right hand side of Equation (4.1) accounts for delayed neutrons. The $c_i(\underline{r},t)$ for i = 1, 2, ..., I are concentrations of delayed neutrons precursors. Since we assume the fuel is stationary, such delayed neutrons appear at point, $\underline{r}$, where the fission took place. Therefore,

$$\int_V K_i(\underline{r},\underline{r}',t)\ c_i(\underline{r}',t)\ dV' = c_i(\underline{r},t);\ \ i = 1, 2, ..., I \qquad (4.4)$$

The behavior of these $c_i(\underline{r},t)$'s is described by Equation (4.2).

The remaining $c_i(\underline{r}',t)$'s, i = I + 1, I + 2, ..., I + J, account for photoneutrons emitted by (γ,n) reactions with nuclei such as deuterium. For these, the neutron is not emitted from the spot at which the γ-ray is released but rather at the spot where the (γ,n) reaction takes place. Thus we introduce for each γ-source, i, (i = I + 1, I + 2, ..., I + J), a "kernel", $K_i(\underline{r},\underline{r}',t)$ with the above definition.

The γ-emitters are of two kinds: those which appear either promptly or after a delay from the fissioning nucleus or its fragments, and those emitted from certain isotopes created when neutrons are captured. The first kind of behavior can be described by Equation (4.2) but with $\beta_i^j\nu$ defined as $\beta_i^j\nu \equiv \gamma_i^j$ that represents the average number of type-i γ-emitters created by fission of isotope-j. For prompt γ's, λ_i is so large that we may set $dc_i/dt = 0$ and introduce $\lambda_i c_i$ from Equation (4.2) directly into Equation (4.1). The concentrations of those $c_i(\underline{r}',t)$'s arising from neutron capture are determined from Equation (4.3).

Next, we integrate Equations (4.1), (4.2), and (4.3) over the volume of an arbitrary node-l to obtain

$$\begin{aligned}\frac{1}{v_g}\frac{d}{dt}\bar{\bar{\varphi}}_g^l(t) = &-\frac{1}{V^l}\sum_{p=1}^{P} A_p \bar{J}_{gp}^l(t) - \bar{\Sigma}_g^l(t)\bar{\bar{\varphi}}_g^l(t) \\ &+ \sum_{g'=1}^{G}\sum_j \frac{1}{\lambda}\chi_{pg}^j(1-\beta^{jl})\nu\bar{\Sigma}_{fg'}^{jl}(t)\bar{\bar{\varphi}}_{g'}^l(t) \\ &+ \sum_{i=1}^{I+J}\chi_{ig}\lambda_i\sum_o \bar{K}_i^{lo}(t)\,\bar{c}_i^o(t) \\ &+ \sum_{\substack{g'=1 \\ g'\neq g}}^{G}\bar{\Sigma}_{gg'}^l(t)\bar{\bar{\varphi}}_{g'}^l(t); \quad g = 1,2,....,G\end{aligned} \tag{4.5}$$

$$\frac{d}{dt}\bar{c}_i^l(t) = \frac{1}{\lambda}\sum_{g'=1}^{G}\sum_j \beta_i^{jl}\nu\bar{\Sigma}_{fg'}^{jl}(t)\bar{\bar{\varphi}}_{g'}^l(t) - \lambda_i\bar{c}_i^l(t); \quad i = 1,2,..., I+J' \tag{4.6}$$

and

$$\frac{d}{dt}\bar{c}_i^l(t) = \sum_{g'=1}^{G}\bar{\Sigma}_{cg'}^{jl}(t)\bar{\bar{\varphi}}_{g'}^l(t) - \lambda_i\bar{c}_i^l(t); \quad i = I+J'+1,..., I+J \tag{4.7}$$

where

V^l ≡ node-l volume,

A_p ≡ face-p area,

l ≡ index representing the node upon which the balance is

performed,

p ≡ an index representing the faces of a node;

p = 1,2,....,P; P being the number of faces, and

$$\bar{J}^{l}_{gp}(t) \equiv \frac{1}{A_p}\int_{A_p} \underline{J}_g(\underline{r},t).\underline{n}_p dA;\ p = 1,2,...,P$$

$$\bar{\bar{\varphi}}^{l}_{g}(t) \equiv \frac{1}{V^l}\int_{V^l} \phi_g(\underline{r},t)dV,$$

$$\bar{\Sigma}^{l}_{g}(t)\bar{\bar{\varphi}}^{l}_{g}(t) \equiv \frac{1}{V^l}\int_{V^l} \Sigma_g(\underline{r},t)\phi_g(\underline{r},t)dV,$$

$$\overline{\nu\Sigma}^{l}_{fg}(t)\bar{\bar{\varphi}}^{l}_{g}(t) \equiv \frac{1}{V^l}\int_{V^l} \nu\Sigma_{fg}(\underline{r},t)\phi_g(\underline{r},t)dV, \qquad (4.8)$$

$$\bar{\Sigma}^{il}_{cg}(t)\bar{\bar{\varphi}}^{l}_{g}(t) \equiv \frac{1}{V^l}\int_{V^l} \Sigma^{i}_{cg}(\underline{r},t)\phi_g(\underline{r},t)dV,$$

$$\bar{\Sigma}^{l}_{gg'}(t)\bar{\bar{\varphi}}^{l}_{g'}(t) \equiv \frac{1}{V^l}\int_{V^l} \Sigma_{gg}(\underline{r},t)\phi_{g'}(\underline{r},t)dV;$$

$$\bar{c}^{l}_{i}(t) \equiv \frac{1}{V^l}\int_{V^l} c_i(\underline{r},t)dV,$$

$$\bar{K}^{lo}_{i}\bar{c}^{o}_{i}(t) \equiv \frac{1}{V^l}\int_{V^l} dV \int_{V^o} K_i(\underline{r},\underline{r}',t)\ c_i(\underline{r}',t)\ dV' .$$

Note that we have assumed that all hexagons have the same cross sectional area, that the node spacing is constant in the plane of the hexagons, and that all nodes have regular geometry so that the face length is the same for all faces. Also, note that according to the definition given above, $\bar{J}^{l}_{gp}$ is the face-averaged current leaving node-l through face p which has an outward-directed normal unit vector $\underline{n}_p$.

As stated before, the objective here is to solve the time-dependent nodal balance equation for the time-dependent volume-averaged fluxes, $\bar{\bar{\varphi}}^{l}_{g'}(t)$.

But as it is obvious from Equation (4.5) we need another relationship between the time-dependent face-averaged currents and the time-dependent volume-averaged flux to be able to reach our goal. This can be attained by using Fick's Law

$$\underline{J}(\underline{r},E,t) \approx -D(\underline{r},E,t)\,\nabla\phi(\underline{r},E,t). \qquad (4.9)$$

This approximation introduces additional unknowns (the time-dependent face-averaged fluxes) to the problem, and the way we are going to deal with those new unknowns will be that outlined in Chapter (2).

To start with, the time-dependent version of Equations (2.20) and (2.21) is

$$J_2^{ij}(t) - \frac{49}{23}J_5^{ij}(t) = -\frac{\overline{D}^{ij}(t)}{h}\left\{-\frac{144}{23}\bar{\varphi}_5^{ij}(t) + \frac{144}{23}\bar{\bar{\varphi}}^{ij}(t)\right\} \qquad (4.10)$$

and

$$\frac{49}{23}J_2^{ij}(t) - J_5^{ij}(t) = -\frac{\overline{D}^{ij}(t)}{h}\left\{+\frac{144}{23}\bar{\varphi}_2^{ij}(t) - \frac{144}{23}\bar{\bar{\varphi}}^{ij}(t)\right\} \qquad (4.11)$$

Also, the only difference (mathematically speaking) between Equation (2.2) and its time-dependent counterpart, Equation (4.5), is that the latter has two additional terms that account for the time evolution of the volume-averaged flux and the contribution to this evolution by the delayed neutrons. This allows us to write down the time-dependent version of Equations (2.22) and (2.23) (for the two-dimensional case) as

$$\frac{1}{v_g}\frac{d}{dt}\bar{\bar{\varphi}}^{l}_{g}(t) + \frac{72}{23}\bar{J}^{l}_{g2}(t) + \sum_{p\neq 2,5}\bar{J}^{l}_{gp}(t) + \bar{\Sigma}^{l}_{g}(t)\bar{\bar{\varphi}}^{l}_{g}(t) =$$

$$\frac{1}{\lambda}\sum_{j}\sum_{g'=1}^{G}\chi^{j}_{gp}(1-\beta^{jl})\overline{\nu\Sigma}^{jl}_{fg'}(t)\bar{\bar{\varphi}}^{l}_{g'}(t) + \sum_{\substack{g'=1\\g'\neq g}}^{G}\bar{\Sigma}^{l}_{gg'}(t)\bar{\bar{\varphi}}^{l}_{g'}(t) \qquad (4.12)$$

$$-\frac{\bar{D}^{l}_{g}}{h}\left\{+\frac{144}{23}\bar{\varphi}^{l}_{g2}(t) - \frac{144}{23}\bar{\bar{\varphi}}^{l}_{g}(t)\right\} + \sum_{i=1}^{I+J}\chi_{ig}\lambda_i\sum_{o}\bar{\bar{K}}^{lo}_{i}(t)\,\bar{c}^{o}_{i}(t)$$

and

$$\frac{1}{v_g}\frac{d}{dt}\bar{\bar{\varphi}}^{m}_{g}(t) + \frac{72}{23}\bar{J}^{m}_{g2}(t) + \sum_{p\neq 2,5}\bar{J}^{m}_{gp}(t) + \bar{\Sigma}^{m}_{g}(t)\bar{\bar{\varphi}}^{m}_{g}(t) =$$

$$\frac{1}{\lambda}\sum_{j}\sum_{g'=1}^{G}\chi^{j}_{gp}(1-\beta^{jm})\overline{\nu\Sigma}^{jm}_{fg'}(t)\bar{\bar{\varphi}}^{m}_{g'}(t) + \sum_{\substack{g'=1\\g'\neq g}}^{G}\bar{\Sigma}^{m}_{gg'}(t)\bar{\bar{\varphi}}^{m}_{g'}(t) \qquad (4.13)$$

$$-\frac{\bar{D}^{m}_{g}}{h}\left\{+\frac{144}{23}\bar{\varphi}^{m}_{g2}(t) - \frac{144}{23}\bar{\bar{\varphi}}^{m}_{g}(t)\right\} + \sum_{i=1}^{I+J}\chi_{ig}\lambda_i\sum_{o}\bar{\bar{K}}^{mo}_{i}(t)\,\bar{c}^{o}_{i}(t)$$

and this will yield, after introducing discontinuity factors in the manner used in the Chapter (2), the time-dependent version of Equation (2.24)

$$\bar{J}^{l}_{g2}(t) = -\bar{J}^{m}_{g5}(t) = \left\{\frac{h}{2}\left[\frac{f^{m}_{g5}}{\bar{\bar{D}}^{m}_{g}(t)} + \frac{f^{l}_{g2}}{\bar{D}^{l}_{g}(t)}\right]\right\}^{-1}\Bigg\{\sum_{p\neq 2,5}^{6}\frac{23h}{144}\left[\bar{J}^{l}_{gp}(t)\frac{f^{l}_{g2}}{\bar{D}^{l}_{g}(t)} - \bar{J}^{m}_{gp}(t)\frac{f^{m}_{g5}}{\bar{\bar{D}}^{m}_{g}(t)}\right]$$

$$+ f^{m}_{g5}\left\{1 - \frac{23h^2}{96\bar{\bar{D}}^{m}_{g}(t)}\left[\frac{1}{v_g}\frac{d}{dt}\bar{\bar{\varphi}}^{m}_{g}(t) + \bar{\Sigma}^{m}_{g}(t)\bar{\bar{\varphi}}^{m}_{g}(t)\right.\right.$$

$$\left.-\frac{1}{\lambda}\sum_{j}\sum_{g'=1}^{G}\chi^{j}_{gp}(1-\beta^{jm})\overline{\nu\Sigma}^{jm}_{fg'}(t)\bar{\bar{\varphi}}^{m}_{g'}(t) - \sum_{i=1}^{I+J}\chi_{ig}\lambda_i\sum_{o}\bar{\bar{K}}^{mo}_{i}(t)\,\bar{c}^{o}_{i}(t) - \sum_{\substack{g'=1\\g'\neq g}}^{G}\bar{\Sigma}^{m}_{gg'}(t)\bar{\bar{\varphi}}^{m}_{g'}(t)\right]\Bigg\}$$

$$- f^{l}_{g2}\left\{1 - \frac{23h^2}{96\bar{D}^{l}_{g}(t)}\left[\frac{1}{v_g}\frac{d}{dt}\bar{\bar{\varphi}}^{l}_{g}(t) + \bar{\Sigma}^{l}_{g}(t)\bar{\bar{\varphi}}^{l}_{g}(t)\right.\right.$$

$$\left.\left.-\frac{1}{\lambda}\sum_{j}\sum_{g'=1}^{G}\chi^{j}_{gp}(1-\beta^{jl})\overline{\nu\Sigma}^{jl}_{fg'}(t)\bar{\bar{\varphi}}^{l}_{g'}(t) - \sum_{i=1}^{I+J}\chi_{ig}\lambda_i\sum_{o}\bar{\bar{K}}^{lo}_{i}(t)\,\bar{c}^{o}_{i}(t) - \sum_{\substack{g'=1\\g'\neq g}}^{G}\bar{\Sigma}^{l}_{gg'}(t)\bar{\bar{\varphi}}^{l}_{g'}(t)\right]\right\}\Bigg\}$$

(4.14)

Substituting this result (along with the analogous expression for the other five currents across the faces of the hexagon) into the nodal balance Equation (4.5) yields an equation coupling the volume-averaged flux in node-l to the volume-averaged fluxes in its six neighbors (m = 1, 2,..., 6). Transverse face-current terms (the summation over p in Equation (4.14) will appear in this "seven-point" nodal equation. These must be updated iteratively using Equation (4.14) and the analogous equations for the other five currents across the node faces. This seven point nodal balance equation will serve, along with Equations (4.6) and (4.7), as the governing equations that give the time evolution of the volume-averaged fluxes of the system.

Although all results obtained above, Equations (4.10 - 14), are for the two-dimensional case (hex), the actual computer code used for the numerical analysis of the proposed nodal model has been written for the one- (z), two- (hex), and three-dimensional (hex-z) cases. The only difference between equations of any two of these geometries is the geometrical coefficients which appear in front of all the terms on the right hand side of Equation (4.14).

Note that discontinuity factors are assumed to be time-independent. The reason for that assumption is based on experience gained from light water reactor transient analysis that has yielded reasonably accurate results when discontinuity factors were taken to be those at the beginning of the transient.

4.3 Thermal-Hydraulic Feedback Model

4.3.1 The WIGL Model

By performing a time-dependent energy balance on the fuel and the coolant in node-l and by assuming that no boiling occurs, the following equations can be derived:

$$\frac{d}{dt}\overline{T}_f^l(t) = \frac{1}{\overline{\rho}_f^l C_f}\left\{(1-r)\,q^l(t) - \frac{V_c^l}{V_f^l}\left[\frac{1}{A_h U} + \frac{1}{A_h h_0\left(\frac{W(t)}{W_0}\right)^{0.8}}\right]^{-1}\left(\overline{T}_f^l(t) - \overline{T}_c^l(t)\right)\right\} \tag{4.15}$$

$$\begin{aligned}\frac{d}{dt}\overline{T}_c^l(t) = \left(\frac{\partial\overline{\rho}_c H}{\partial\overline{T}_c}\right)^{-1}\{\,& r\,q^l(t)\frac{V_f^l}{V_c^l} + \left[\frac{1}{A_h U} + \frac{1}{A_h h_0\left(\frac{W(t)}{W_0}\right)^{0.8}}\right]^{-1}\left(\overline{T}_f^l(t) - \overline{T}_c^l(t)\right) \\ & + \frac{2W_c^l(t)C_c}{V_c^l}\left(\overline{T}_i^l(t) - \overline{T}_c^l(t)\right)\}\end{aligned} \tag{4.16}$$

and

$$\overline{T}_i^l(t) = 2\overline{T}_c^m(t) - \overline{T}_i^m(t) \tag{4.17}$$

where

$\overline{T}_f^l(t)$ ≡ time-dependent average fuel temperature in node-*l*,

$\overline{T}_c^l(t)$ ≡ time-dependent average coolant temperature in node-*l*,

$\overline{T}_i^l(t)$ ≡ time-dependent inlet coolant temperature of node-*l*,

r ≡ fraction of fission power which is deposited directly into coolant,

$\left(\frac{\partial\overline{\rho}_c H}{\partial\overline{T}_c}\right)$ ≡ energy required to raise the average temperature of a unit volume of coolant by one temperature unit,

$q^l(t)$ ≡ volumetric energy generation rate in node-*l*,

V_c^l ≡ volume of coolant in node-*l*,

V_f^l ≡ volume of fuel in node-*l*,

A_h ≡ total heat transfer area/total coolant volume within a node,

h_0 ≡ heat transfer coefficient,

U ≡ conductivity/conduction lengths of the fuel, gap, and cladding(i.e., the inverse of the resistance of heat flow),

C_c ≡ specific heat of the coolant,

C_f ≡ specific heat of the fuel,

$\overline{\rho_f}^l$ ≡ average fuel density in node-l,

$\overline{\rho_c}^l$ ≡ average coolant density in node-l,

W_0 ≡ total coolant mass flow rate into core at time = 0,

$W(t)$ ≡ time-dependent total coolant mass floe rate into core,

$W_c^l(t)$ ≡ time-dependent coolant mass flow rate through node-l.

The above three equations are solved directly for the two unknowns; the time-dependent average coolant temperature, the time-dependent average fuel temperature for all nodes in the reactor. Then, the time-dependent average coolant density is evaluated for all nodes using FLOWTRAN, a subroutine that utilizes explicit correlations based on the average coolant temperatures with uniform pressure assumed throughout the reactor core.

4.3.2 Cross Section Feedback

Feedback from the thermal-hydraulic equations to the neutronic equations is accomplished by assuming that all macroscopic cross sections (and inverse diffusion coefficients) are linear functions of the three-hydraulic variables. That is, the cross sections are assumed to obey equations of the form

$$\overline{\Sigma_\alpha}^l(t) = \overline{\Sigma_\alpha}^{l^*} + \frac{\partial\overline{\Sigma_\alpha}}{\partial\overline{T_c}}\left(\overline{T_c}^l(t) - \overline{T_c}^*\right) + \frac{\partial\overline{\Sigma_\alpha}}{\partial\overline{T_f}}\left(\overline{T_f}^l(t) - \overline{T_f}^*\right) + \frac{\partial\overline{\Sigma_\alpha}}{\partial\overline{\rho_c}}\left(\overline{\rho_c}^l(t) - \overline{\rho_c}^*\right) \qquad (4.18)$$

where the starred quantities refer to references conditions. In the next chapter a description of a numerical procedure to incorporate the feedback option in the solution will be given.

4.4 Summary

The goal of this chapter was to derive the time-dependent, three-dimensional (hex-z), few-group nodal diffusion equations with thermal-hydraulic feedback option. An arbitrary number of energy groups and upscattering in thermal groups were allowed for. Finally, a simple, time-dependent, constant pressure, one-dimensional (parallel channel) thermal-hydraulic model was described. Numerical methods for solving the time-dependent nodal balance equations with a thermal-hydraulic feedback option will be discussed in next chapter.

CHAPTER FIVE

NUMERICAL SOLUTION METHOD FOR THE DYNAMIC NEUTRON DIFFUSION EQUATION AND APPLICATIONS

5.1 Introduction

In Chapter(4), the time-dependent, three-dimensional (hex-z), few-group nodal diffusion equations with thermal hydraulic feedback option were derived. The remaining tasks are: 1) develop a numerical solution method by which these equations can be solved, and 2) apply the proposed nodal method to benchmark problems for evaluation and verification purposes.

Prior to writing the time-dependent governing equations of the nodal model in a matrix form, the time derivative of both the volume-averaged flux and the concentrations of the delayed neutron precursors have to be approximated numerically. To accomplish this, the fission source in the delayed neutron precursor equations is assumed to vary linearly with time which makes these equations analytically solvable. Then, for the neutron equations, a fully implicit method with a truncation error of order $O(\Delta t)$ is used for its unconditional stability. This will yield a set of linear equations that have the same shape as those of the static part of the problem mentioned in Chapter (3). This will prompt the use of a numerical method solution

similar to what was used for the solution of the static diffusion nodal balance equation as described in Chapter (3). Next, the theory will be applied to one-(z) and three-dimensional (hex-z) cores using a two-group analysis which includes upscattering from the thermal group with thermal-hydraulic feedback option.

5.2 Numerical Properties

If we assume that the fission source on the right hand side of Equation (4.6) (the same applies to Equation (4.7)) varies linearly with time, we can solve Equation (4.6) analytically as follows

$$\lambda_i \bar{c}_{in}^{l} = e^{-\lambda_i \Delta t_n} \lambda_i \bar{c}_{in-1}^{l} + \left(1 - \theta_{in} - e^{-\lambda_i \Delta t_n}\right) \sum_j \beta_i^{jl} \bar{S}_{n-1}^{jl} + \theta_{in} \sum_j \beta_i^{jl} \bar{S}_n^{jl} \qquad (5.1)$$

where n is the time index reflecting the value of the variable in question at time t, whereas n - 1 reflects its value at time t - Δt, and

$$\theta_{in} = \frac{e^{-\lambda_i \Delta t_n} - \left(1 - \lambda_i \Delta t_n\right)}{\lambda_i \Delta t_n},$$

$$\Delta t_n = t_n - t_{n-1}, \text{ and}$$

$$\bar{S}_n^{jl} = \frac{1}{\lambda} \sum_{g'=1}^{G} \nu \bar{\Sigma}_{fg'n}^{jl} \bar{\bar{\varphi}}_{g'n}^{l}. \qquad (5.2)$$

Now, if we substitute this result into Equation (4.5) and use a fully implicit expression to approximate the flux time derivative we get the following:

$$\frac{1}{v_g}\frac{\bar{\bar{\varphi}}^{l}_{gn} - \bar{\bar{\varphi}}^{l}_{gn-1}}{\Delta t_n} = -\frac{1}{V^{l}}\sum_{p=1}^{P} A_p \bar{J}^{l}_{gpn} - \bar{\Sigma}^{l}_{gn}\bar{\bar{\varphi}}^{l}_{gn} + \sum_{\substack{g'=1 \\ g'\neq g}}^{G} \bar{\Sigma}^{l}_{gg'n}\bar{\bar{\varphi}}^{l}_{g'n}$$

$$+ \sum_{i=1}^{I+J} \chi_{ig}\, e^{-\lambda_i \Delta t_n}\lambda_i \bar{c}^{l}_{in-1} + \chi_{ig}\left(1 - \theta_{in} - e^{-\lambda_i \Delta t_n}\right)\sum_j \beta_i^{jl}\bar{S}^{jl}_{n-1} \qquad (5.3)$$

$$+ \chi_{ig}\theta_{in}\sum_j \beta_i^{jl}\bar{S}^{jl}_{n} + \sum_j \chi^{j}_{pg}(1-\beta^{jl})\bar{S}^{jl}_{n} \quad ; \quad g = 1,2,....,G$$

A close look at Equation (5.3) shows that it is similar in structure to Equation (2.2), the static nodal balance equation, except that the former has a source term that consists of values of all the variables at a prior time step (n - 1). Also, $(v_g\Delta t_n)^{-1}$ is added to the removal macroscopic cross section in Equation (2.2) and the fission source term is modified to account for delayed neutrons emission.

Note that if Equation (4.7) is used instead of Equation (4.6) to account for the emission of other types of delayed neutrons, the only difference that this change will bring about is the use of the capture cross section instead of the fission cross section, in Equation (5.3), along with the corresponding neutron yield that goes with it.

If we follow the procedure outlined in Chapter (2) from introducing the quadratic approximation up to defining the discontinuity factors and finally eliminating the face-averaged fluxes, but use Equation (5.3) in order to eliminate the unwanted face-averaged currents, we will get an expression for the face-averaged currents analogous to Equation (2.24). For the two-dimensional case we will have

$$\bar{J}^{l}_{g2n} = -\bar{J}^{m}_{g5n} = \{\frac{h}{2}[\frac{f^{m}_{g5}}{\bar{D}^{m}_{gn}} + \frac{f^{l}_{g2}}{\bar{D}^{l}_{gn}}]\}^{-1}\{\sum_{p\neq 2,5}^{6}\frac{23h}{144}[\bar{J}^{l}_{gpn}\frac{f^{l}_{g2}}{\bar{D}^{l}_{gn}} - \bar{J}^{m}_{gpn}\frac{f^{m}_{g5}}{\bar{D}^{m}_{gn}}]$$

$$+ f^{m}_{g5}\{1 - \frac{23h^2}{96\bar{D}^{m}_{gn}}[\left(\frac{1}{v_g\Delta t_n} + \bar{\Sigma}^{m}_{gn}\right)\bar{\bar{\varphi}}^{m}_{gn} - \sum_{j}\left[\sum_{i=1}^{I+J}\chi_{ig}\theta_{in}\beta_i^{jm} + \chi^{j}_{pg}(1-\beta^{jm})\right]\bar{\bar{S}}^{jm}_{n}$$

$$- \left(\bar{Q}^{l}_{n-1} + \sum_{\substack{g'=1\\ g'\neq g}}^{G}\bar{\Sigma}^{m}_{gg'n}\bar{\bar{\varphi}}^{m}_{g'n}\right)]\} \qquad (5.4a)$$

$$- f^{l}_{g2}\{1 - \frac{23h^2}{96\bar{D}^{l}_{gn}}[\left(\frac{1}{v_g\Delta t_n} + \bar{\Sigma}^{l}_{gn}\right)\bar{\bar{\varphi}}^{l}_{gn} - \sum_{j}\left[\sum_{i=1}^{I+J}\chi_{ig}\theta_{in}\beta_i^{jl} + \chi^{j}_{pg}(1-\beta^{jl})\right]\bar{\bar{S}}^{jl}_{n}$$

$$- \left(\bar{Q}^{l}_{n-1} + \sum_{\substack{g'=1\\ g'\neq g}}^{G}\bar{\Sigma}^{l}_{gg'n}\bar{\bar{\varphi}}^{l}_{g'n}\right)]\}\}$$

where $\bar{Q}^{l}_{n-1}$ is the source term that contains values of all the variables at the time step (n - 1) for node-*l*.

Substituting this result (along with the analogous expression for the other five currents across the faces of the hexagon) into the nodal balance Equation (5.3) yields an equation coupling the volume-averaged flux in node-*l* to the volume-averaged fluxes in its six neighbors (m = 1, 2,..., 6). Transverse face-current terms (the summation over p in Equation (2.24) will appear in this "seven-point" ("nine-point" in the case of hex-z geometry) nodal equation. These must be updated iteratively using Equation (5.4) and the analogous equations for the other five currents across the node faces.

There is an alternative way to eliminate the unwanted face-averaged currents from the time-dependent nodal balance equation. Instead of approximating the volume-averaged flux time derivative with a fully implicit finite-difference expression, as in Equation (5.3), we rather substitute for the time derivative of the volume-averaged flux in Equation (4.5) and the delayed

neutron precursor concentrations in Equations (4.6) and (4.7) the inverse period multiplied by the volume-averaged flux and the delayed neutron precursor concentrations at time step (n) respectively. The volume-averaged flux and the delayed neutron precursor concentrations are assumed to vary exponentially with time, and hence their inverse periods can be defined as

$$[\omega_n]^{(t+1)} \equiv \frac{[\phi_n]^{(t+1)} - [\phi_{n-1}]}{\Delta t_n}$$

and

$$[\omega_{in}]^{(t+1)} \equiv \frac{[C_{in}]^{(t+1)} - [C_{in-1}]}{\Delta t_n}$$

Then, if we follow the procedure outlined in Chapter (2) from introducing the quadratic approximation up to defining the discontinuity factors and finally eliminating the face-averaged fluxes, the face-averaged current equation will then look like:

$$\begin{aligned}
\bar{J}^l_{g2n} = -\bar{J}^m_{g5n} = \{&\frac{h}{2}\left[\frac{f^m_{g5}}{\bar{D}^m_{gn}} + \frac{f^l_{g2}}{\bar{D}^l_{gn}}\right]\}^{-1}\{\sum_{p\neq 2,5}^{6}\frac{23h}{144}\left[\bar{J}^l_{gpn}\frac{f^l_{g2}}{\bar{D}^l_{gn}} - \bar{J}^m_{gpn}\frac{f^m_{g5}}{\bar{D}^m_{gn}}\right]\\
&+ f^m_{g5}\{1 - \frac{23h^2}{96\bar{D}^m_{gn}}\left[\left(\frac{\bar{\omega}^m_{gn}}{v_g} + \bar{\Sigma}^m_{gn}\right)\bar{\bar{\varphi}}^m_{gn} - \sum_j\left[\sum_{i=1}^{I+J}\frac{\lambda_i\chi_{ig}\beta_i^{jm}}{\bar{\omega}^m_{in}+\lambda_i} + \chi^j_{pg}(1-\beta^{jm})\right]\bar{\bar{S}}^{jm}_n\right.\\
&\left. - \left(\bar{Q}^l_{n-1} + \sum_{\substack{g'=1\\g'\neq g}}^{G}\bar{\Sigma}^m_{gg'n}\bar{\bar{\varphi}}^m_{g'n}\right)\right]\}\\
&- f^l_{g2}\{1 - \frac{23h^2}{96\bar{D}^l_{gn}}\left[\left(\frac{\bar{\omega}^l_{gn}}{v_g} + \bar{\Sigma}^l_{gn}\right)\bar{\bar{\varphi}}^l_{gn} - \sum_j\left[\sum_{i=1}^{I+J}\frac{\lambda_i\chi_{ig}\beta_i^{jl}}{\bar{\omega}^l_{in}+\lambda_i} + \chi^j_{pg}(1-\beta^{jl})\right]\bar{\bar{S}}^{jl}_n\right.\\
&\left. - \left(\bar{Q}^l_{n-1} + \sum_{\substack{g'=1\\g'\neq g}}^{G}\bar{\Sigma}^l_{gg'n}\bar{\bar{\varphi}}^l_{g'n}\right)\right]\}\}
\end{aligned} \tag{5.4b}$$

The reason for using this expression for the face-averaged current rather than equation (5.4a) is that the former assumes that the volume-averaged flux and the precursor concentrations vary exponentially with time whereas the latter assumes that these two variables vary linearly with time. For certain situations, this is a more realistic approximation for both the volume-averaged flux and precursor concentrations which then eliminates the first order truncation error associated with the linear approximation.

Substituting this result (along with the analogous expression for the other five currents across the faces of the hexagon) into the time-dependent nodal balance yields an equation coupling the volume-averaged flux in node-l to the volume-averaged fluxes in its six neighbors (m = 1, 2,..., 6). Transverse face-current terms (the summation over p in Equation (2.24) will appear in this "seven-point" ("nine-point" in the case of hex-z geometry) nodal equation. These must be updated iteratively using Equation (5.4b) and the analogous equations for the other five currents across the node faces.

To evaluate the face-averaged currents using Equation (5.4b), the volume-averaged fluxes have to be determined, first to evaluate the inverse periods and the delayed neutron precursor concentrations. But to evaluate the volume-averaged fluxes (and the delayed neutron precursor concentrations), the inverse periods have to be known first. A way out of this problem, is to use the latest available inverse periods (from the last outer iteration) to determine the volume-averaged fluxes; then use these flux values to determine the delayed neutron precursor concentrations and the inverse periods. The resultant values are used to determine the face-averaged currents from equation (5.4b).

Another way to overcome the above problem is to substitute algebraically Equation (5.4a) into Equation (5.3) to get the volume-averaged fluxes (and the delayed neutron precursor concentrations) at time step n. Then, use these values to determine the inverse periods for Equation (5.4b).

Now, we are ready to write down the time-dependent governing equations in a matrix form so that an appropriate numerical solution method can be devised. These equations are

$$[A'''] [\phi_n] = [M'''] [\phi_n] + [C'] [J_n] + [Q_{n-1}] \tag{5.5}$$

and

$$[J_n] = [C'] [J_n] + [X] [\phi_n] + [X'] [Q_{n-1}] \tag{5.6}$$

where [A'''], [M'''], [C'], [X], and [X'] are square matrices and of order N*G and $[\phi_n]$, $[J_n]$, and $[Q_{n-1}]$ are column vectors of dimension N*G. In the next section a iteration scheme to solve Equations (5.5) and (5.6) numerically will be outlined.

5.3 Numerical Solution Scheme

The method that will be used to solve Equations (5.5) and (5.6) is the same used to solve Equations (3.10) and (3.11) and consists of three layers of iteration: fission source iterations, flux iterations, and current iterations. Acceleration techniques will be used for fission source iterations and for flux iterations while current iterations will remain unaccelerated for reasons that will be pointed out in the coming sections.

Since the proposed numerical scheme has already been explained in Chapter (3), we shall not describe it in detail. Instead, we shall give a summary of the iterative method to highlight the difference between the static and the transient problems.

Summary of the Iterative Method

A flow diagram of the iterative method is given in Figure (5.1). The general iterative scheme proceeds as follows

1. An initial guess is made for the flux vector $[\phi_n]^{(t)}$ at time step (n). (Usually $[\phi_{n-1}]$).
2. From this guess the fission source is calculated.
3. Several flux (usually one per fission source iteration) iterations are performed to calculate a new flux vector $[\phi_n]^{(t+1)}$.
4. The new delayed neutron precursor concentrations are calculated using the new flux vector.
5. The inverse period for both the volume-averaged flux and the delayed neutron concentrations are calculated.
6. Several current (usually one per fission source iteration) iterations are performed to calculate a new current vector $[J_n]^{(t+1)}$ (Using Equation (5.4b)).
7. With the new flux and current vectors, we repeat the process starting with step 2 until the flux vector converges.

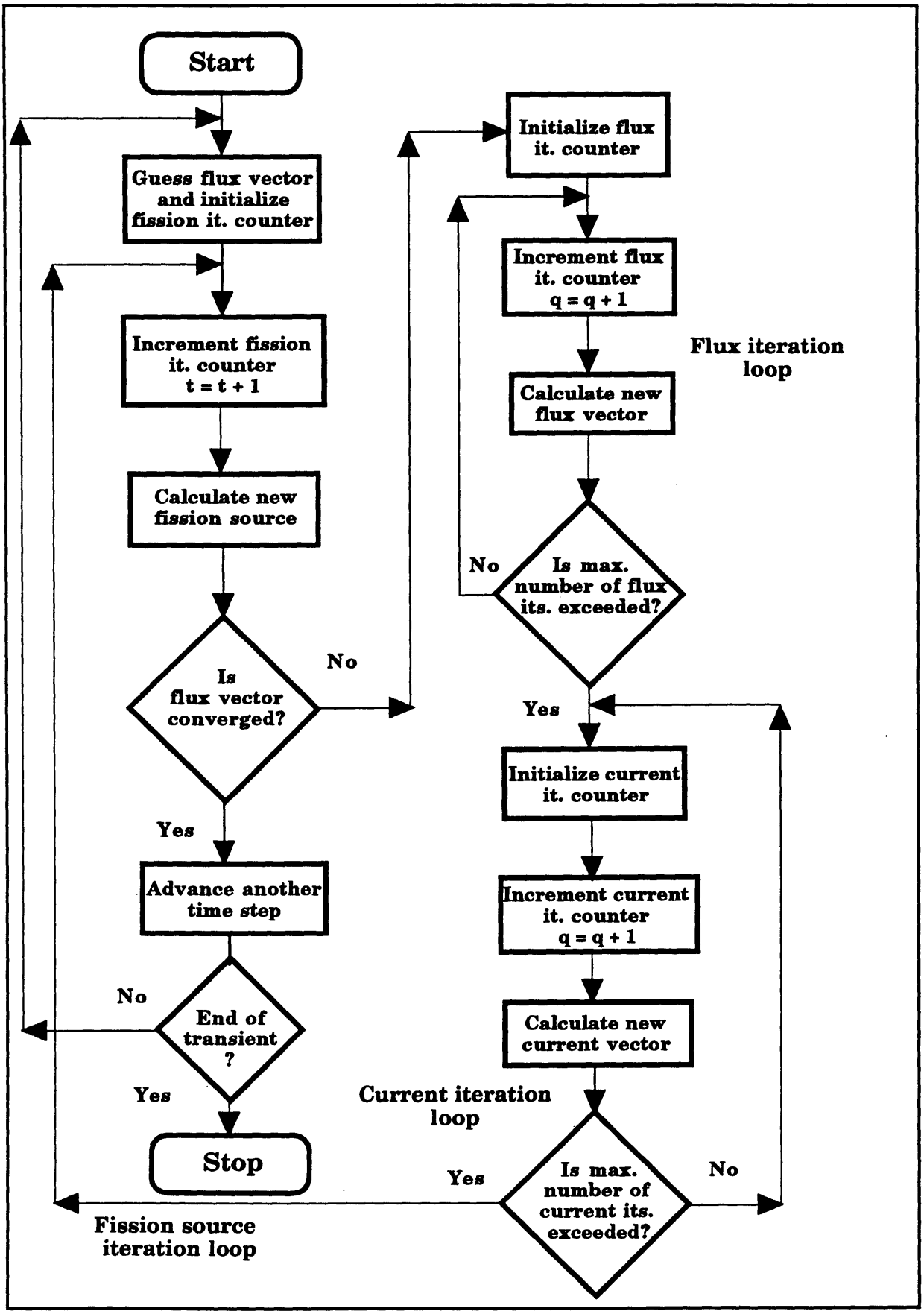

Figure (5.1) Flow diagram of iterative solution method.

8. Update the nuclear cross sections according to the new converged flux vector (If thermal-hydraulic feedback option is chosen).
9. Start a new time step (n + 1) and repeat the process starting with step 1 until the transient ends.

5.4 Applications

The accuracy of the nodal model described in the preceding sections has been tested numerically by comparison with a number of reference calculations. The transient option of the computer code ' **MITHEX-Z** ' solves transient problems taking initial conditions from the static part of the same code. The result of these numerical tests will be presented under two sets of applications; 1) applications involve problems without thermal-hydraulic feedback, and 2) applications involve problems with thermal-hydraulic feedback.

5.4.1 Applications without Thermal-Hydraulic Feedback

The largest of these tests, designated as the Joshua problem, involved a three-dimensional (hex-z), two-group simulation of a heavy water reactor of the Savannah River type. Figure (5.2) gives an overview of one-sixth of a cross sectional area of the reactor. From the figure, we can see that the core is composed of homogenized hexagons (about 18 cm across flats) and has 60^0-degree rotational symmetry. Also, the core is heterogeneous in the z-direction but is symmetric around the mid-plane. It has zero-flux boundary condition in both axial and transverse directions. The transient analyzed involved a step reduction of the thermal removal cross section of the central

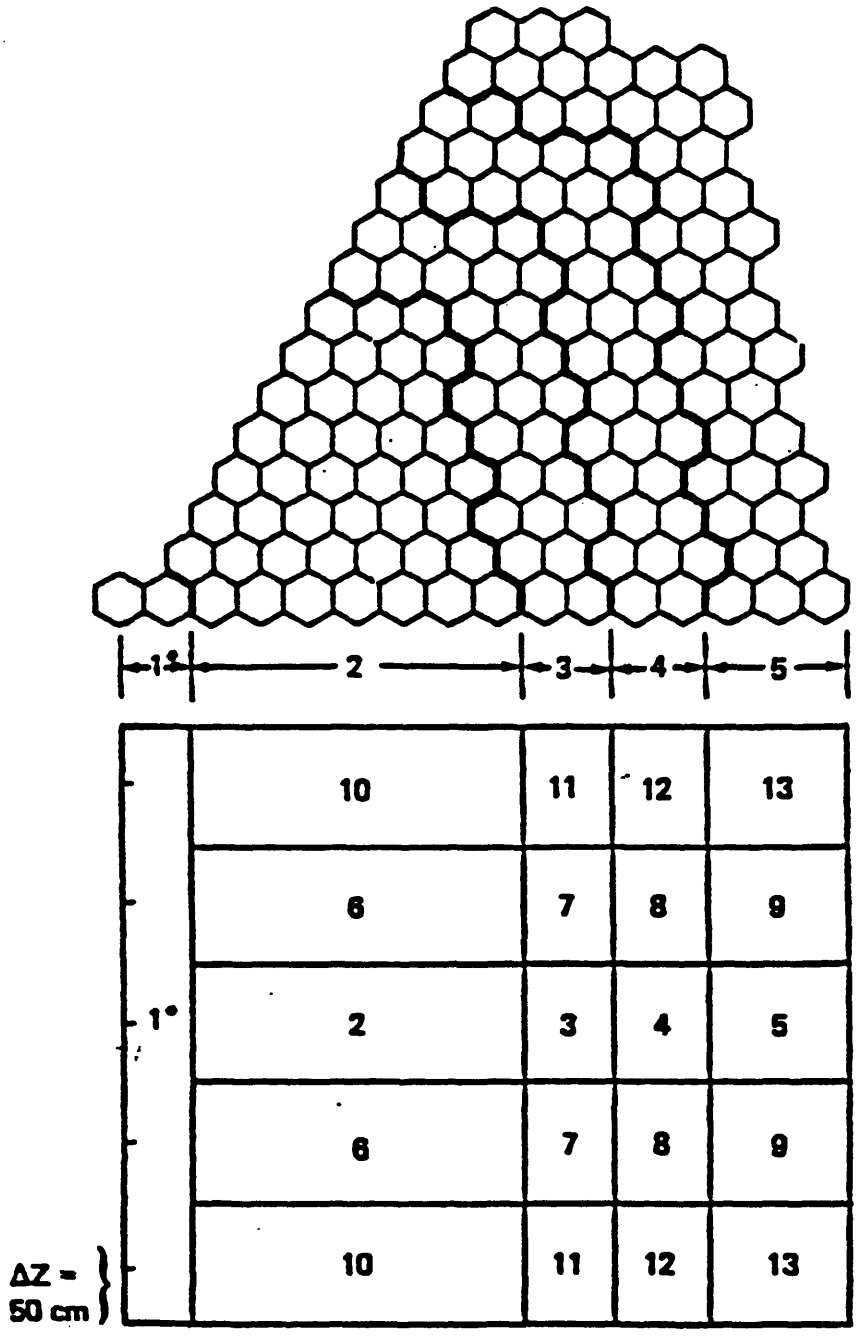

Figure (5.2) Reactor geometry for the Joshua test(60-deg sector at midplane and axial cross section of the reactor)- (From Buckner et al., 1976).

patch (seven hexagons in the center of the core) by 15% at time t = 0. Material specifications and core dimensions are given in Appendix B. Figure (5.3) shows the normalized thermal flux at the central hexagon as a function of time compared to results published earlier (Buckner, 1976).

As can be seen from Figure (5.3), **MITHEX-Z** shows consistency in predicting the core behavior when the number of axial segments is increase from 5 to 10. However, the model underpredicts the thermal flux as compared with Buckner's results. This may be due to the spectral approximation used by Buckner et al. **MITHEX-Z** took about one day (clock time on IBM RISC/6000) to calculate the transient. This lengthy running time is attributed to the fact that the whole core was analyzed (not one-sixth) and to the relatively large number of unknowns per node per energy group which is inherent in the model.

To test further the accuracy of the quadratic model, a much smaller three-dimensional benchmark problem was analyzed. The core is the same as the one that is shown in Figure (3.4) but with a total height of 200 cm. Material specifications and properties are given in Appendix B.

The first test involved inputting as initial conditions the steady state eigenvalue, fluxes and currents along with the steady state cross sections. The code maintained the core steady state as expected. Second, the code was given perturbed fluxes and current but with the steady state eigenvalue and cross sections. The solution went back to a steady state condition as expected. Finally, the core was set on a period of 10 s. by giving it a steady state eigenvalue that corresponded to that of a core with the same geometry

and material compositions but with a increased removal cross section. The amount of that increase was equal to $(0.1/v_g)$ where v_g is the group-g neutron velocity. The core followed the prescribed period asymptotically after one hour (clock time on IBM RSIC/6000).

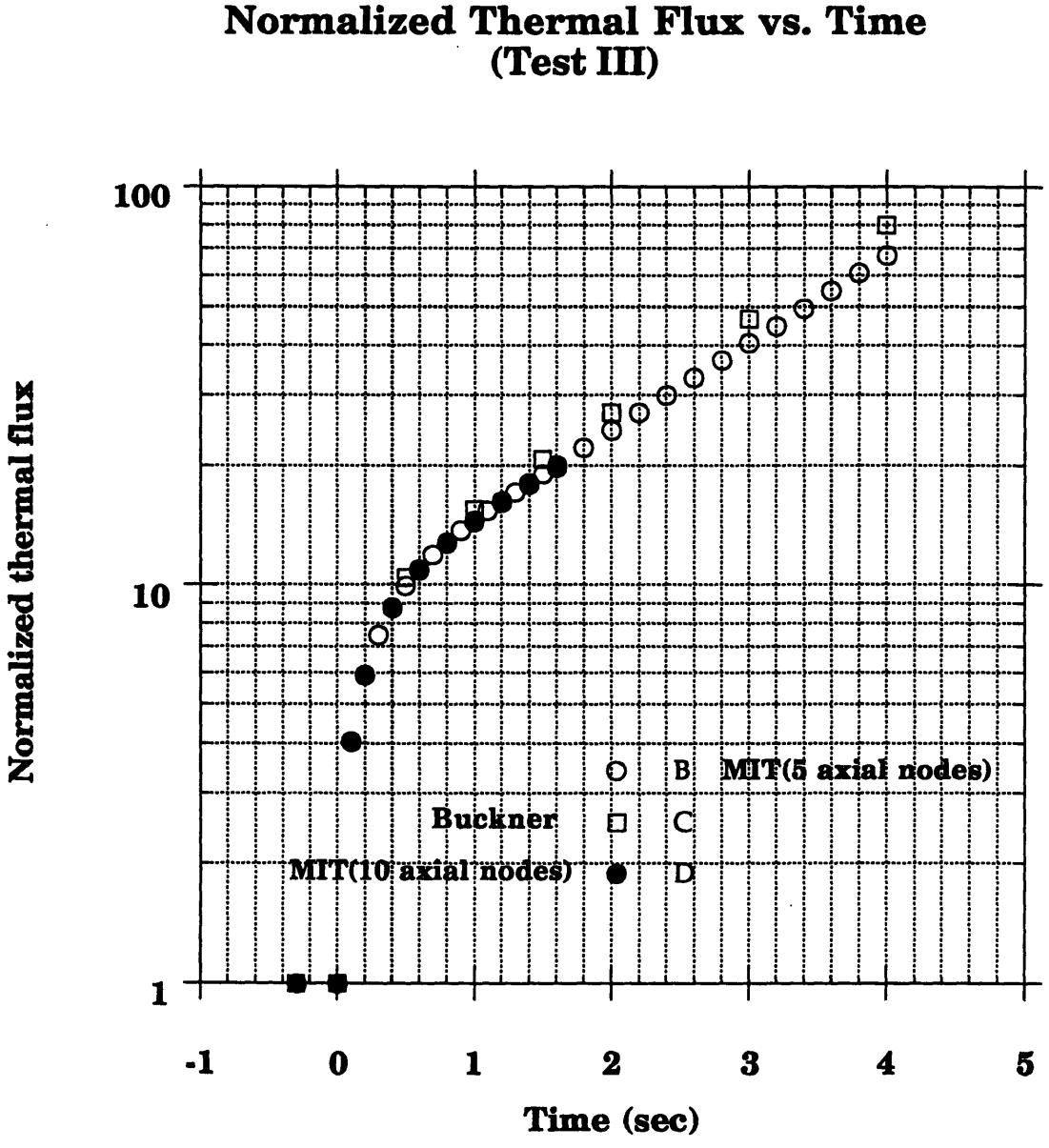

Figure (5.3) Normalized thermal flux vs. time for Joshua problem.

Here, we do not have any reference execution time to compare with, however, we believe that the inherent relatively large number of unknowns per node

per energy groups of the simplified quadratic model increases the overall execution time of the code.

5.4.2. Application with Thermal-Hydraulic Feedback

The one-dimensional problem tested in Chapter (3) was run for a transient with thermal-hydraulic feedback option and slightly different macroscopic cross sections and thermal-hydraulic feedback parameters. These constants are given in Appendix B. The transient involved a step decrease in the inlet coolant temperature by 20 F^0 degrees. Figure (5.4) shows the history of the total power of the core which started at 2.4 MWt at time t = 0 compared to results from CONQUEST (Gehin, 1992). Execution time for **MITHEX-Z** was 70 s (on IBM RSIC/6000) and 54 s for CONQUEST (on DEC 3100). Although we can not draw a definite conclusion regarding the speed difference between the two codes (different machines, different time steps, different solution method, and frequency of cross section updating) there is definitely a room for improvement in the overall performance of **MITHEX-Z** with respect to problem execution time.

We conclude from this test that the time-dependent thermal-hydraulic feedback component of the code is working as expected and provides good agreement with one-dimensional benchmark results. Note that there is practically nothing in the public literature about either steady state or transient thermal-hydraulic feedback benchmark problems for heavy water reactors of Savannah River type. The reason for this goes back to the nature of the applications for which those reactors are used.

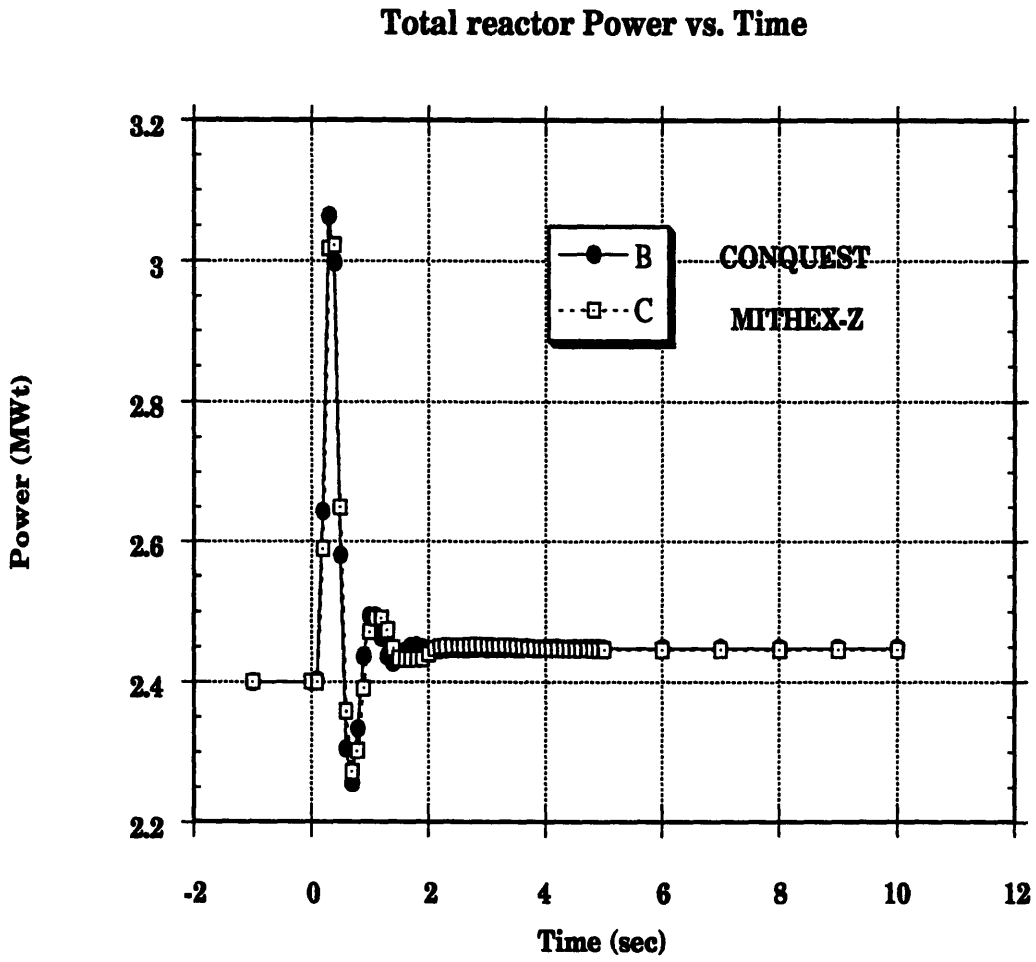

Figure (5.4) 20-F^0-degree decrease in the coolant inlet temperature.

5.5 Summary

In Chapter(4), the time-dependent, three-dimensional (hex-z), few-group nodal diffusion equations incorporating a thermal hydraulic feedback option were derived. In the present chapter a numerical solution method by which these equations can be solved has been developed, and results have been applied to benchmark problems for evaluation and verification purposes.

These tests show that the time-dependent thermal-hydraulic feedback component of the code is working correctly.

CHAPTER SIX

SUMMARY AND CONCLUSIONS

6.1 Summary

The objective of this research was to develop and implement a method for analyzing three-dimensional static and transient behavior of reactors composed of regular hexagonal subregions in radial planes. The intent was to develop a nodal code in hex-z geometry capable of solving few-group diffusion equations that predict the static as well as the transient behavior of node-averaged group-fluxes. A simple, constant pressure, one-dimensional (parallel channel) thermal-hydraulic model was also incorporated into the code.

In Chapter (2) the static, three-dimensional (hex-z), few-group nodal diffusion equations with thermal-hydraulic feedback option were derived. Also, a separate two-dimensional, few-group, finite-difference nodal diffusion model for triangular-shaped nodes was outlined. The triangular-shaped nodes were required for the calculation of discontinuity factors and for obtaining a fine-mesh, finite difference solution to serve as a reference. These discontinuity factors were needed to correct for errors due to nodal-homogenization, the use of diffusion theory and the quadratic approximation

of the face-averaged fluxes. In the triangular-shaped-node model the transverse-averaged fluxes are assumed to have a flat shape across the node, whereas in the hexagonal-shaped-node model they are assumed to have a quadratic one. In addition, we allowed for a general number of energy groups and for upscattering in thermal groups. Finally, a simple, constant pressure, one-dimensional (parallel channel) thermal-hydraulic model was incorporated.

The numerical properties of the nodal diffusion equations for both the triangular and the hexagonal models were discussed in Chapter (3). An iterative scheme was devised and the computer code ' **MITHEX-Z** ' was applied to benchmark problems in one-, two-, and three-dimensional geometries. The code accuracy was good compared to benchmark problem results. However, it has a relatively long execution time and the primary reason for this being the relatively large number of unknowns per node per energy group.

In Chapter (4), the time-dependent, three-dimensional (hex-z), few-group nodal diffusion equations with a thermal-hydraulic feedback option were derived. We allowed for a general number of energy groups and for upscattering in thermal groups. Finally, a simple, constant pressure, one-dimensional (parallel channel) thermal-hydraulic model was incorporated.

The numerical properties of the time-dependent nodal diffusion equations for the hexagonal model were discussed in Chapter (5). An iterative scheme was devised and was applied to benchmark problems in one-

and three-dimensional geometries. Again, the accuracy was good but the execution time was relatively large.

6.2 Conclusions and Recommendations

The simple quadratic nodal method provides a substantial improvement over the finite-difference method with one mesh box per hexagon. In fact, the quadratic model is proved to be more accurate and faster than the finite-difference model with 6 triangles/hex. Whether homogenized cross sections and discontinuity factors found from infinite lattice calculations provide acceptable accuracy for the quadratic model remains an open question. The thermal-hydraulic feedback component, both static and dynamic, is working properly and provides results which agree with those of one-dimensional benchmark problems employing the same equations.

Although there has not been any definitive comparison to show how fast ' **MITHEX-Z** ' is, we believe that there is much to be done to achieve improved computational speed. To begin with, the current model involves 9 unknowns per node per energy group, 8 of which are face-averaged currents. This makes the code spends most of its computational time in determining the face-averaged currents. Hence, an effort has to be made, either to reduce the number of these unknowns or to compute them more quickly. Also, a rotational symmetry option should be added to the code so that having to solve for the whole core for symmetric problems can be avoided.

Faster acceleration schemes for both the fission source and the flux iterations should be explored and implemented. Numerical properties that govern the convergence properties of these two iteration schemes should be investigated and analyzed to find out the most efficient acceleration method.

The nonlinear iteration scheme introduced into recent nodal codes in r-z and x-y-z geometries (Byers, 1992 and Gehin, 1992) should be explored and, if attractive, implemented. Finally, a quasi-static model for solving the time-dependent neutron diffusion equations should speed up the overall performance of the code.

REFERENCES

Buckner, M.R. and Stewart, J.W., "Multidimensional Space-Time Nuclear-Reactor Kinetics Studies - Part I: Theoretical", *Nuclear Science and Engineering*, **59**, 289-297 (1976).

Byers, M.E., "A Transient Nodal Method for Reactor Models in R-Z Geometry", Ph.D.. Thesis, Department of Nuclear Engineering, M.I.T., Cambridge, Massachusetts (September, 1992).

Cadwell, W.R., "PDQ-7: A Program for the Solution of the Neutron Diffusion Equations in Two Dimensions", WAPD-TM-678, Bettis Atomic Power Laboratory (1967).

Delp, D.L. et al., "FLARE - A Three-Dimensional Boiling Water Reactor Simulator", GEAP-4598 (July 1964).

Finnemann, H. and Wagner, M.R., "A New Computational Technique for the Solution of Multidimensional Neutron Diffusion Problems", presented at the International Meeting of Specialists on Methods of Neutron Transport Theory in Reactor Calculations, Bologna, Italy (November, 1975).

Gehin, J.C., "A Nodal Method for the Solution of the Static, Few-Group Diffusion Equations in Hexagonal Geometry", M.Sc. Thesis, Department of Nuclear Engineering, M.I.T., Cambridge, Massachusetts (February, 1990).

Gehin, J.C., "A Quasistatic Polynomial Nodal Method for Nuclear Reactor Analysis", Ph.D.. Thesis, Department of Nuclear Engineering, M.I.T., Cambridge, Massachusetts (September, 1992).

Hageman, L.A. and Young, D.M., *Applied Iterative Methods*, Academic Press, San Diego, California (1981).

Henry, A.F., *Nuclear Reactor Analysis*, M.I.T. Press, Cambridge, Massachusetts (1975).

Koebke, K., "A New Approach to Homogenization and Group Consolidation", paper presented at the IAEA Technical Committee Meeting on Homogenization Method in Reactor Physics, Lugano, Switzerland (November 1978).

Lawrence, R.D. and Dorning, J.J., "A Nodal Green's Function Method for Multidimensional Neutron Diffusion Calculations", *Trans. Am. Nucl. Soc.*, **28**, 248-249 (1978).

Lawrence, R.D., " A Nodal Method for Three-Dimensional Fast Reactor Calculations in Hexagonal Geometry", Proceedings of the ANS Topical Meeting on Advances in Reactor Computation, Salt Lake City, Utah (March, 1983).

Lawrence, R.D., "The DIF3D Nodal Neutronics Option for Two- and Three-Dimensional Diffusion Theory Calculations in Hexagonal Geometry", Argonne National Laboratory, Argonne, Illinois, ANL-83-1 (March, 1983).

Nakamura, S., *Computational Methods in Engineering and Science with Applications to Fluid Mechanics and Nuclear Systems*, John Wiley & Sons, New York (1986).

Shatilla, Y.A. and Henry, A.F., "A Simple Quadratic Nodal Model for Hexagonal Geometry", Proceedings of the ANS Topical Meeting on Advances in Reactor Physics, Charleston, South Carolina (March 1992).

Smith, K.S., "An Analytical Nodal Model for Solving the Two-Group, Multidimensional, Static and Transient Neutron Diffusion Equations", N.E. and M.Sc. Thesis, Department of Nuclear Engineering, M.I.T., Cambridge, Massachusetts (March, 1979).

Smith, K.S., "Spatial Homogenization Methods for Light Water Reactor Analysis", Ph.D. Thesis, Department of Nuclear Engineering, M.I.T., Cambridge, Massachusetts (June, 1980).

Taiwo, T.A. and Khalil, H.S., "An Improved Quasistatic Option for the DIF3D Nodal Kinetics Code", Proceedings of the ANS Topical Meeting on Advances in Reactor Physics, Charleston, South Carolina (March 1992).

Taiwo, T.A. and Khalil, H.S., "The DIF3D Nodal Kinetics Capability in Hexagonal-Z Geometry -- Formulation and Preliminary Tests", Proceedings of

the International Topical Meeting on Advances in Mathematics, Computations and Radiation Shielding, and Reactor Physics, Pittsburgh, Pennsylvania (April 1991).

Varga, R.S., *Matrix Iterative Analysis*, Prentice-Hall, Englewood Cliffs, New Jersey, (1962).

Vota, A.V., Curlee, Jr., N.J., and Henry, A.F., "WIGL3 - A Program for the Steady State and Transient Solution of the One-Dimensional, Two-Group, Space-Time Diffusion Equations Accounting for Temperature, Xenon, and Control Feedback", WAPD-TM-788 (February 1969).

Wachspress, E.L., *Iterative Solution to Elliptic Systems and Applications to the Neutron Diffusion Equations of Reactor Physics*, Prentice-Hall, Englewood Cliffs, New Jersey (1966).

Wagner, M.R., "Three Dimensional Nodal Diffusion and Transport Theory Methods for Hexagonal-Z Geometry", *Nuclear Science and Engineering*, **103**, 377-391 (1989).

Yarman, F.A., "Analytic Nodal Theory in Hexagonal Geometry", Ph.D. Thesis, Department of Nuclear Engineering, M.I.T., Cambridge, Massachusetts (October, 1983).

Zerkle, M.L., "Development of A Polynomial Nodal Method with Flux and Current Discontinuity Factors", Ph.D. Thesis, Department of Nuclear Engineering, M.I.T., Cambridge, Massachusetts (June, 1992).

APPENDIX A

MATERIAL SPECIFICATIONS (Static Applications)

A.1 Applications without Thermal-Hydraulic Feedback

A.1.1 ANL-Mark22 Problem

The core height is 381 cm and the material specifications are given in Table (A.1). All discontinuity factors are taken to be unity.

Table (A.1) Group cross sections for ANL-Mark22 problem.

Mat. #	Group (g)	Diff.	Fiss.	Prod.	Scat. from g	Rem.
1	1	1.2742	0.0	0.0	$1.29322*10^{-2}$	$1.35165*10^{-2}$
	2	0.85689	0.0	0.0	$1.55259*10^{-5}$	$1.15155*10^{-2}$
2	1	1.3484	$1.0561*10^{-3}$	$2.579*10^{-3}$	$7.83449*10^{-3}$	$1.04796*10^{-2}$
	2	0.86326	$1.0836*10^{-2}$	$2.6366*10^{-2}$	$2.05684*10^{-5}$	$2.24906*10^{-2}$
4	1	1.2742	0.0	0.0	$1.29322*10^{-2}$	$1.35165*10^{-2}$
	2	0.85689	0.0	0.0	$1.55259*10^{-5}$	$1.10155*10^{-2}$
5	1	1.2742	0.0	0.0	$1.29322*10^{-2}$	$1.35165*10^{-2}$
	2	0.85689	0.0	0.0	$1.55259*10^{-5}$	$2.51552*10^{-3}$
6	1	1.3461	$1.0789*10^{-3}$	$2.6339*10^{-3}$	$8.06868*10^{-3}$	$1.07802*10^{-2}$
	2	0.87207	$1.0842*10^{-2}$	$2.638*10^{-2}$	$2.30825*10^{-5}$	$8.06868*10^{-3}$

7	1	1.2482	0.0	0.0	$1.3685*10^{-2}$	$1.07802*10^{-2}$
	2	0.84707	0.0	0.0	0.0	$7.2945*10^{-5}$
8	1	1.25929	0.0	0.0	$1.12824*10^{-2}$	$1.25649*10^{-2}$
	2	0.836855	0.0	0.0	$1.8482*10^{-5}$	$1.79703*10^{-2}$
9	1	0.6616	0.0	0.0	$1.5811*10^{-2}$	$2.0464*10^{-2}$
	2	0.283	0.0	0.0	0.0	$1.2404*10^{-1}$
11	1	1.2742	0.0	0.0	$1.29322*10^{-2}$	$1.35165*10^{-2}$
	2	0.85689	0.0	0.0	$1.55259*10^{-5}$	$1.52155*10^{-2}$
12	1	1.2742	0.0	0.0	$1.29322*10^{-2}$	$1.35165*10^{-2}$
	2	0.85689	0.0	0.0	$1.55259*10^{-5}$	$1.33155*10^{-2}$
13	1	1.2742	0.0	0.0	$1.29322*10^{-2}$	$1.35165*10^{-2}$
	2	0.85689	0.0	0.0	$1.55259*10^{-5}$	$9.91552*10^{-3}$

A.1.2 Two-Dimensional Smaller Problems

Material specifications for both homogeneous and heterogeneous problems are given in Tables (A.2-5).

Table (A.2) Heterogeneous group cross sections for the two-dimensional problems.

Mat.	Group (g)	Diff.	Fiss.	Prod.	Scat. from g	Rem.
C	1	1.42322	0.0	0.0	$2.48468*10^{-2}$	$2.64234*10^{-2}$
	2	0.95460	0.0	0.0	$1.34505*10^{-4}$	$2.17498*10^{-2}$
M	1	1.2900	0.0	0.0	$8.0000*10^{-3}$	$8.02913*10^{-3}$
	2	0.8830	0.0	0.0	0.0	$7.96268*10^{-3}$
F	1	1.60065	$3.81577*10^{-3}$	$9.3291*10^{-3}$	$2.90765*10^{-3}$	$1.67614*10^{-2}$
	2	1.00857	$1.23103*10^{-1}$	$2.9953*10^{-1}$	$3.55199*10^{-4}$	$1.76437*10^{-1}$
T	1	0.80496	$3.32233*10^{-3}$	$6.1283*10^{-3}$	$6.68233*10^{-3}$	$2.79203*10^{-2}$
	2	0.867324	$2.0605*10^{-2}$	$5.0136*10^{-2}$	$3.55199*10^{-4}$	$7.7294*10^{-2}$

M ≡ Moderator and reflector; C ≡ Control; F ≡ Fuel; T ≡ Target.

Table (A.3) Homogenized group cross sections for the two-dimensional problems.

Mat.	Group (g)	Diff.	Fiss.	Prod.	Scat. from g	Rem.
C	1	1.31919	0.0	0.0	$1.16912*10^{-2}$	$1.20594*10^{-2}$
	2	0.901342	0.0	0.0	$3.44566*10^{-5}$	$5.63097*10^{-3}$
F	1	1.38504	$1.16741*10^{-3}$	$2.8542*10^{-3}$	$6.44203*10^{-3}$	$8.86506*10^{-3}$
	2	0.898526	$1.52191*10^{-3}$	$3.7031*10^{-2}$	$4.39128*10^{-5}$	$2.18825*10^{-2}$
T	1	1.17097	$5.69905*10^{-4}$	$1.5039*10^{-3}$	$6.68233*10^{-3}$	$1.29105*10^{-2}$
	2	0.880244	$3.62256*10^{-3}$	$8.8144*10^{-3}$	$3.55199*10^{-4}$	$1.36547*10^{-2}$

C ≡ Control; F ≡ Fuel; T ≡ Target.

Table (A.4) Discontinuity factors for the two-dimensional heterogeneous problem.

Face	Gr. (g)	Control	Fuel	Target
1	1	0.885373	0.911467	1.02478
	2	1.07866	1.41692	1.11079
2	1	1.16916	0.927869	0.898176
	2	1.01053	1.23505	1.21855
3	1	0.885373	0.904496	1.06441
	2	1.07866	1.22472	1.04198
4	1	1.16916	0.941519	0.936213
	2	1.01053	1.06817	1.16806
5	1	0.885373	0.924038	1.02274
	2	1.07866	1.16567	1.06240
6	1	1.16916	0.913307	0.913401
	2	1.01053	1.15798	1.23035

Table (A.5) Discontinuity factors for the two-dimensional homogeneous problem.

Face	Gr. (g)	Control	Fuel	Target
1	1	0.858707	0.975408	1.03509
	2	1.10407	1.19461	0.972797
2	1	1.15601	1.00217	0.905985
	2	0.982936	1.00978	1.10956
3	1	0.858707	1.01040	1.08484
	2	1.10407	1.00414	0.913804
4	1	1.15601	1.09665	0.958337
	2	0.982936	0.875806	1.03711
5	1	0.858707	1.04456	1.03518
	2	1.10407	0.952904	0.933542
6	1	1.15601	1.01220	0.922531
	2	0.982936	0.950889	1.10200

A.1.3 One-Dimensional Problem

All discontinuity factors are taken to be unity.

Table (A.5) Homogenized group cross sections for the one-dimensional problems.

Mat.	Group (g)	Diff.	Fiss.	Prod.	Scat. from g	Rem.
F	1	1.38504	$1.16741*10^{-3}$	$2.8542*10^{-3}$	$6.44203*10^{-3}$	$8.86506*10^{-3}$
	2	0.898526	$1.52191*10^{-3}$	$3.7031*10^{-2}$	$4.39128*10^{-5}$	$2.18825*10^{-2}$
T	1	1.17097	$5.69905*10^{-4}$	$1.5039*10^{-3}$	$6.68233*10^{-3}$	$1.29105*10^{-2}$
	2	0.880244	$3.62256*10^{-3}$	$8.8144*10^{-3}$	$3.55199*10^{-4}$	$1.36547*10^{-2}$

F ≡ Fuel; T ≡ Target.

A.2 Applications with Thermal-Hydraulic Feedback

A.2.1 Three-Dimensional Smaller Problem

Nuclear macroscopic cross sections are the same for the homogenized two-dimensional problems in Section (A.1.2). All discontinuity factors are taken to be unity. All the partial derivatives with respect to coolant density are taken to be zero.

Total reactor power = 24.0 MWt.

Energy conversion factor = $3.2*10^{-11}$ Joules/fission.

Specific heat of coolant = $5.43*10^{7}$ ergs/(gm*K^0).

Conduction length = $2.2*10^{6}$ ergs/(cm^2*K^0*s).

Heat transfer coefficient at initial flow = $2.71*10^{7}$ ergs/(cm^2*K^0*s).

Fraction of energy released in coolant = 0.0.

Core inlet temperature = 300.0 K^0.

Core flow rate = 3.0 kg/s/node.

Core pressure = 15.3 MPa.

Density of fuel (target) = 10.3 g/cm^3.

Fuel reference temperature = 500.0 K^0.

Coolant reference temperature = 300.0 K^0.

Coolant reference density = 1.0 gm/cm^3.

Coolant volume fraction = 0.363784.

Surface area of clad/coolant of volume = 4.54444 cm^{-1}.

Table (A.6) Partial derivatives with respect to fuel temperature.

Mat.	Group (g)	Diff.$^{-1}$	Fiss.	Prod.	Scat. from g	Capt..
F	1	$-2.6*10^{-6}$	$5.000*10^{-8}$	$3.000*10^{-8}$	$-8.500*10^{-8}$	$3.300*10^{-7}$
	2	$-2.6*10^{-6}$	$1.000*10^{-7}$	$2.430*10^{-7}$	$8.000*10^{-10}$	$3.800*10^{-9}$
T	1	$-1.6*10^{-6}$	$5.000*10^{-8}$	$5.000*10^{-8}$	$-8.500*10^{-8}$	$-3.300*10^{-8}$
	2	$-2.6*10^{-6}$	$7.000*10^{-8}$	$2.430*10^{-7}$	$8.000*10^{-10}$	$1.800*10^{-7}$

F ≡ Fuel; T ≡ Target.

Table (A.7) Partial derivatives with respect to coolant temperature.

Mat.	Group (g)	Diff.$^{-1}$	Fiss.	Prod.	Scat. from g	Capt..
F	1	$-8.0*10^{-5}$	$-5.000*10^{-8}$	$-5.000*10^{-7}$	$-5.500*10^{-7}$	$-3.000*10^{-7}$
	2	$-1.3*10^{-4}$	$-8.300*10^{-7}$	$-2.017*10^{-6}$	$7.000*10^{-8}$	$-5.200*10^{-7}$
T	1	$-8.0*10^{-5}$	$-5.00*10^{-8}$	$-5.000*10^{-7}$	$-5.500*10^{-7}$	$-3.000*10^{-8}$
	2	$-1.3*10^{-4}$	$-8.30*10^{-7}$	$-2.017*10^{-6}$	$7.000*10^{-8}$	$-5.200*10^{-7}$

F ≡ Fuel; T ≡ Target.

A.2.2 One-Dimensional Problem

Material cross sections are the same given in Section (A.1.3). All discontinuity factors are taken to be unity. All the partial derivatives with respect to coolant density are taken to be zero.

Total reactor power = 2.40 MWt.

Energy conversion factor = $3.2*10^{-11}$ Joules/fission.

Conduction length = $2.2*10^{6}$ ergs/(cm^2*K^0*s).

Heat transfer coefficient at initial flow = $2.71*10^{7}$ ergs/(cm^2*K^0*s).

Fraction of energy released in coolant = 0.0.

Core inlet temperature = 300.0 K^0.

Core flow rate = 3.0 kg/s.

Core pressure = 15.3 MPa.

Fuel reference temperature = 500.0 K^0.

Coolant reference temperature = 300.0 K^0.

Coolant reference density = 1.0 gm/cm^3.

Coolant volume fraction = 0.363784.

Surface area of clad/coolant of volume = 4.54444 cm^{-1}.

Table (A.8) Partial derivatives with respect to fuel temperature.

Mat.	Group (g)	Diff.$^{-1}$	Fiss.	Prod.	Scat. from g	Capt..
F	1	$-2.6*10^{-6}$	$5.000*10^{-8}$	$3.000*10^{-8}$	$-8.500*10^{-8}$	$3.300*10^{-7}$
	2	$-2.6*10^{-6}$	$1.000*10^{-7}$	$2.430*10^{-7}$	$8.000*10^{-10}$	$3.800*10^{-9}$
T	1	$-1.6*10^{-6}$	$5.000*10^{-8}$	$5.000*10^{-8}$	$-8.500*10^{-8}$	$-3.300*10^{-8}$
	2	$-2.6*10^{-6}$	$7.000*10^{-8}$	$2.430*10^{-7}$	$8.000*10^{-10}$	$1.800*10^{-7}$

F ≡ Fuel; T ≡ Target.

Table (A.9) Partial derivatives with respect to coolant temperature.

Mat.	Group (g)	Diff.$^{-1}$	Fiss.	Prod.	Scat. from g	Capt..
F	1	$-8.0*10^{-5}$	$-5.000*10^{-8}$	$-5.000*10^{-7}$	$-5.500*10^{-7}$	$-3.000*10^{-7}$
	2	$-1.3*10^{-4}$	$-8.300*10^{-7}$	$-2.017*10^{-6}$	$7.000*10^{-8}$	$-5.200*10^{-7}$
T	1	$-8.0*10^{-5}$	$-5.00*10^{-8}$	$-5.000*10^{-7}$	$-5.500*10^{-7}$	$-3.000*10^{-8}$
	2	$-1.3*10^{-4}$	$-8.30*10^{-7}$	$-2.017*10^{-6}$	$7.000*10^{-8}$	$-5.200*10^{-7}$

F ≡ Fuel; T ≡ Target.

APPENDIX B

MATERIAL SPECIFICATIONS (Transient Applications)

B.1 Applications without Thermal-Hydraulic Feedback

B.1.1 Joshua Problem

The core height is 250 cm and the material specifications are given in Table (B.1). All discontinuity factors are taken to be unity.

Table (B.1) Group cross sections for Joshua problem.

Mat. #	Group (g)	Diff.	Fiss.	Velocity	Scat. from g	Rem.
1	1	1.370	$8.1665*10^{-4}$	∞	$1.00*10^{-2}$	$1.300*10^{-2}$
	2	0.840	$6.1249*10^{-3}$	$5.00*10^{6}$	0.0	b

a: All materials have the same macroscopic cross sections except for the thermal removal cross sections.
b: Thermal cross sections for different materials are given in Table (B.2).

ν = 2.43 neutrons/fission

Number of precursor groups = 1

Precursor constants: $\lambda_1 = 0.1$ sec^{-1} , $\beta_1 = 0.0065$, $\chi_1^1 = 1.0$ and $\chi_1^2 = 0.0$

Table (B.2) Thermal removal cross section for different materials.

Mat. #	Rem.	Mat. #	Rem.
1	$1.355*10^{-2}$	8	$1.325*10^{-2}$
2	$1.355*10^{-2}$	9	$1.320*10^{-2}$
3	$1.350*10^{-2}$	10	$1.315*10^{-2}$
4	$1.345*10^{-2}$	11	$1.310*10^{-2}$
5	$1.340*10^{-2}$	12	$1.305*10^{-2}$
6	$1.335*10^{-2}$	13	$1.300*10^{-2}$
7	$1.330*10^{-2}$		

B.1.2 Three-Dimensional Smaller Problems

Nuclear macroscopic cross sections are the same for the homogenized two-dimensional problems in Section (A.1.2). All discontinuity factors are taken to be unity. Precursor constants are given in Table (B.3).

Fast group neutron velocity = $1.0*10^7$ cm/s.

Thermal group neutron velocity = $3.0*10^5$ cm/s.

Table (B.3) Precursor constants for the three-dimensional smaller problems.

	Fuel		Target	
Gr.	λ_i	β_i	λ_i	β_i
1	$1.27*10^{-2}$	$2.66*10^{-4}$	$1.27*10^{-2}$	$2.85*10^{-4}$
1	$1.27*10^{-2}$	$2.66*10^{-4}$	$1.27*10^{-2}$	$2.85*10^{-4}$
1	$1.27*10^{-2}$	$2.66*10^{-4}$	$1.27*10^{-2}$	$2.85*10^{-4}$
1	$1.27*10^{-2}$	$2.66*10^{-4}$	$1.27*10^{-2}$	$2.85*10^{-4}$
1	$1.27*10^{-2}$	$2.66*10^{-4}$	$1.27*10^{-2}$	$2.85*10^{-4}$
1	$1.27*10^{-2}$	$2.66*10^{-4}$	$1.27*10^{-2}$	$2.85*10^{-4}$

B.1 Applications with Thermal-Hydraulic Feedback

Material cross sections are the same given in Section (A.1.3). All discontinuity factors are taken to be unity. All the partial derivatives with respect to coolant density are taken to be zero.

Fast group neutron velocity = $1.0*10^7$ cm/s.

Thermal group neutron velocity = $3.0*10^5$ cm/s.

Number of precursor groups = 1

Precursor constants: $\lambda_1 = 1.4$ sec^{-1} , $\beta_1 = 0.00096$ $\chi_1^1 = 1.0$ and $\chi_1^2 = 0.0$

Total reactor power = 2.40 MWt.

Energy conversion factor = $3.204*10^{-11}$ Joules/fission.

Specific heat of coolant = $5.43*10^7$ ergs/(gm*K^0).

Conduction length = $2.2*10^6$ ergs/(cm^2*K^0*s).

Heat transfer coefficient at initial flow = $2.71*10^7$ ergs/(cm^2*K^0*s).

Fraction of energy released in coolant = 0.0.

Core inlet temperature = 300.0 K^0.

Core flow rate = 3.0 kg/s.

Core pressure = 15.3 MPa.

Density of fuel (target) = 10.3 g/cm^3.

Fuel reference temperature = 500.0 K^0.

Coolant reference temperature = 300.0 K^0.

Coolant reference density = 1.0 gm/cm^3.

Coolant volume fraction = 0.363784.

Surface area of clad/coolant of volume = 4.54444 cm^{-1}.

Derivative of density*enthalpy w.r.t. coolant temperature = $1.60*10^7$ ergs/(cm^3*K^0).

Table (B.4) Partial derivatives with respect to fuel temperature.

Mat.	Group (g)	Diff.$^{-1}$	Fiss.	Prod.	Scat. from g	Capt..
F	1	$-2.6*10^{-6}$	$5.000*10^{-8}$	$3.000*10^{-8}$	$-8.500*10^{-8}$	$3.300*10^{-7}$
	2	$-2.6*10^{-6}$	$1.000*10^{-7}$	$2.430*10^{-7}$	0.0	$3.800*10^{-9}$
T	1	$-1.6*10^{-6}$	$5.000*10^{-8}$	$5.000*10^{-8}$	$-8.500*10^{-8}$	$-3.300*10^{-8}$
	2	$-2.6*10^{-6}$	$7.000*10^{-8}$	$2.430*10^{-7}$	0.0	$1.800*10^{-7}$

F ≡ Fuel; T ≡ Target.

Table (B.5) Partial derivatives with respect to coolant temperature.

Mat.	Group (g)	Diff.$^{-1}$	Fiss.	Prod.	Scat. from g	Capt..
F	1	$-8.0*10^{-5}$	$-5.000*10^{-8}$	$-5.000*10^{-7}$	$-5.500*10^{-7}$	$-3.000*10^{-7}$
	2	$-1.3*10^{-4}$	$-8.300*10^{-7}$	$-2.017*10^{-6}$	0.0	$-5.200*10^{-7}$
T	1	$-8.0*10^{-5}$	$-5.00*10^{-8}$	$-5.000*10^{-7}$	$-5.500*10^{-7}$	$-3.000*10^{-8}$
	2	$-1.3*10^{-4}$	$-8.30*10^{-7}$	$-2.017*10^{-6}$	0.0	$-5.200*10^{-7}$

F ≡ Fuel; T ≡ Target.